Evolution of the Adria-Europe plate boundary in the northern Dinarides: From continent-continent collision to back-arc extension

Kamil Ustaszewski,[1,2] Alexandre Kounov,[1] Stefan M. Schmid,[3,4] Urs Schaltegger,[5] Erwin Krenn,[6] Wolfgang Frank,[7,8] and Bernhard Fügenschuh[9]

Received 18 January 2010; revised 13 July 2010; accepted 18 August 2010; published 28 December 2010.

[1] The Sava Zone of the northern Dinarides is part of the Cenozoic Adria-Europe plate boundary. Here Late Cretaceous subduction of remnants of Meliata-Vardar oceanic lithosphere led to the formation of a suture, across which upper plate European-derived units of Tisza-Dacia were juxtaposed with Adria-derived units of the Dinarides. Late Cretaceous siliciclastic sediments, deposited on the Adriatic plate, were incorporated into an accretionary wedge that evolved during the initial stages of continent-continent collision. Structurally deeper parts of the exposed accretionary wedge underwent amphibolite-grade metamorphism. Grt-Pl-Ms-Bt thermobarometry and multiphase equilibria indicate temperatures between 550°C and 630°C and pressures between 5 and 7 kbar for this event. Peak metamorphic conditions were reached at around 65 Ma. Relatively slow cooling from peak metamorphic conditions throughout most of the Paleogene was possibly induced by hanging wall erosion in conjunction with southwest directed propagation of thrusting in the Dinarides. Accelerated cooling took place in Miocene times, when the Sava Zone underwent substantial extension that led to the exhumation of the metamorphosed units along a low-angle detachment. Footwall exhumation started under greenschist facies conditions and was associated with top-to-the-north tectonic transport, indicating exhumation from below European plate units. Extension postdates the emplacement of a 27 Ma old granitoid that underwent solid-state deformation under greenschist facies conditions. The $^{40}Ar/^{39}Ar$ sericite and zircon and apatite fission track ages from the footwall allow bracketing this extensional unroofing between 25 and 14 Ma. This extension is hence linked to Miocene rift-related subsidence in the Pannonian basin, which represents a back-arc basin formed due to subduction rollback in the Carpathians. **Citation:** Ustaszewski, K., A. Kounov, S. M. Schmid, U. Schaltegger, E. Krenn, W. Frank, and B. Fügenschuh (2010), Evolution of the Adria-Europe plate boundary in the northern Dinarides: From continent-continent collision to back-arc extension, *Tectonics*, *29*, TC6017, doi:10.1029/2010TC002668.

1. Introduction

1.1. Plate Tectonic Setting and Aims of This Study

[2] The eastern Mediterranean Dinarides-Hellenides orogen (Figure 1) formed by the collision of the Adriatic plate with Europe-derived units at the end of the Cretaceous, whereby Adria came to reside in a lower plate position. Final collision was preceded by plate convergence since the Late Jurassic and the progressive closure of the intermittent Neotethys Ocean [e.g., *Channell and Horváth*, 1976; *Channell et al.*, 1979; *Burchfiel*, 1980; *Dercourt et al.*, 1986; *Ricou et al.*, 1986]. Substantial postcollisional strike-slip overprint related to Neogene northward motion of the Adriatic plate [e.g., *Csontos and Vörös*, 2004; *Ustaszewski et al.*, 2008] and a widespread Neogene cover render the plate boundary between Adria and Europe one of the most obscure parts of the Dinarides-Hellenides orogen. This study focuses on the northernmost part of this plate boundary along the northern end of the internal Dinarides, adjacent to the southwestern margin of the Pannonian basin.

[3] This plate boundary zone was first described as "Sava-Vardar Zone" [*Pamić*, 1993a, 2002]. *Schmid et al.* [2008] termed the same area "Sava Zone" in order to distinguish it from the Vardar Zone (western Vardar Ophiolitic Unit of *Schmid et al.* [2008]), which hosts widespread ophiolites in the Dinarides and Hellenides. These Triassic-Jurassic-age ophiolites were obducted onto the distal Adriatic passive margin during the latest Jurassic to earliest Cretaceous [*Aubouin et al.*, 1970; *Pamić and Hrvatović*, 2000]. The Sava Zone formed by the final closure of this Mesozoic northern branch of Neotethys (Meliata-Maliac-Vardar Ocean of *Schmid et al.* [2008]) (also including the Maliac Ocean of *Stampfli and Borel* [2002]); no trace of a so-called Pindos Ocean is documented from the Dinarides. The Sava Zone separates Adria-derived thrust sheets, i.e., the Dinarides, from the northerly and easterly adjacent Europe-derived

[1]Institute of Geology and Paleontology, University of Basel, Basel, Switzerland.
[2]Now at Lithosphere Dynamics, GFZ German Research Centre for Geosciences, Potsdam, Germany.
[3]Department of Earth Sciences, Freie Universität Berlin, Berlin, Germany.
[4]Institute of Geophysics, ETH Zurich, Zurich, Switzerland.
[5]Department of Mineralogy, University of Geneva, Geneva, Switzerland.
[6]Division of Mineralogy, Department of Materials Science and Physics, University of Salzburg, Salzburg, Austria.
[7]Central European Argon Laboratory, Geological Institute, Slovak Academy of Sciences, Bratislava, Slovakia.
[8]Institute for Geology, University of Vienna, Vienna, Austria.
[9]Geological-Paleontological Institute, Innsbruck, Austria.

0278-7407/10/2010TC002668

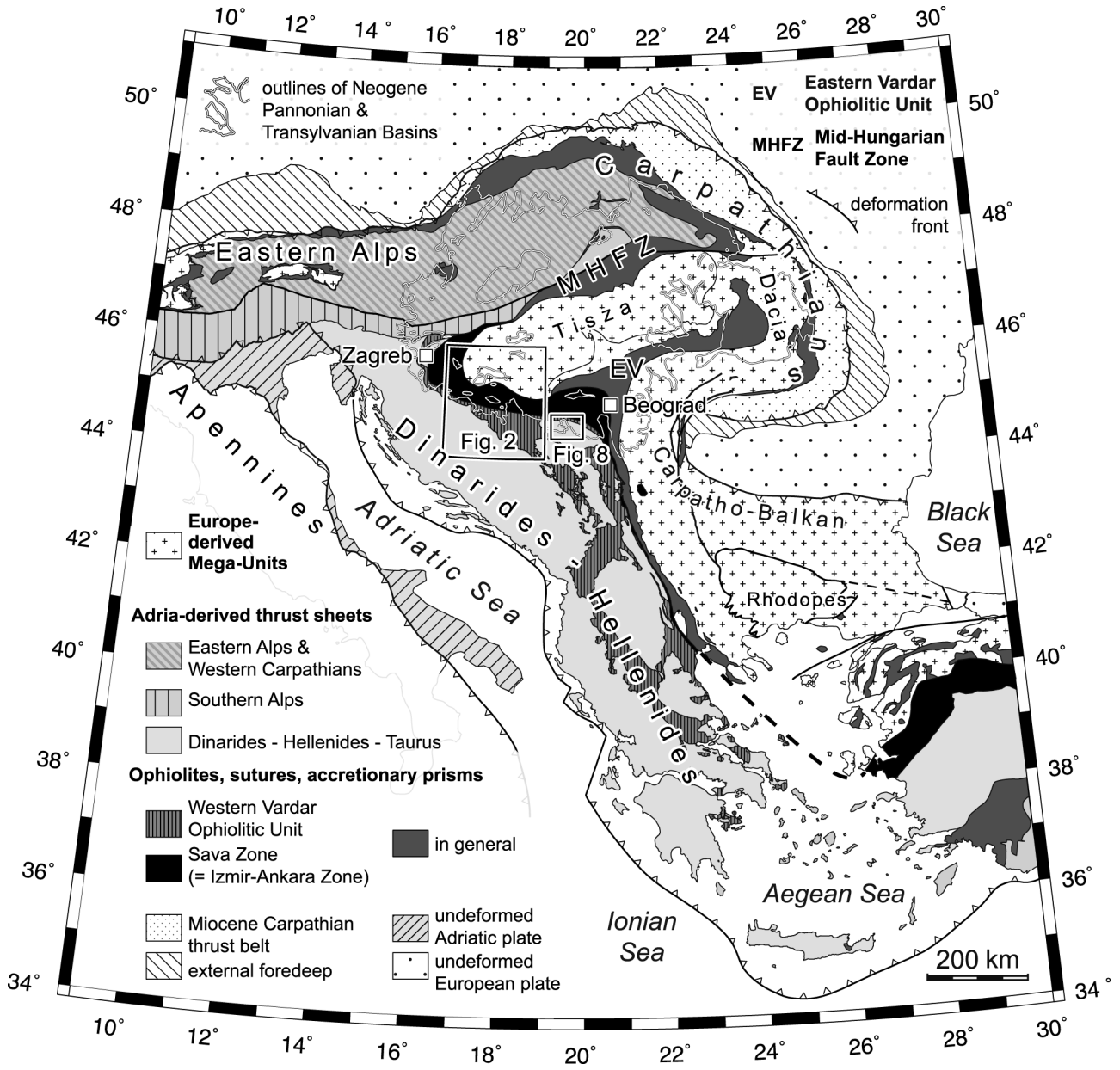

Figure 1. Major tectonic units of the Alps, Carpathians, Dinarides, and Hellenides (north of 42°N; simplified after *Schmid et al.* [2008]).

Tisza and Dacia Mega-unit occupying an upper plate position [*Haas*, 2001; *Haas and Péró*, 2004] (Figure 1). The Tisza-Dacia Mega-unit represents a composite continental terrane assembled in the Late Cretaceous ("Tisza-Dacia terrane" of *Csontos and Vörös* [2004]). Since these units originally broke off the European plate in the Jurassic [e.g., *Săndulescu*, 1984] they may be considered a part of the European plate for the sake of simplicity.

[4] The Sava Zone contains post-Variscan rocks metamorphosed up to the amphibolite facies. Our study concentrates on the most complete transect across this suture in northern Bosnia and Croatia, reaching from upper plate European units to lower plate Adria-derived units, including previously obducted Neotethyan ophiolites. Other regionally metamorphosed assemblages in the Dinarides associated with the Sava Zone lie in western and southern Serbia [*Marović et al.*, 2007a, 2007b; *Schefer et al.*, 2007, 2008; *Zelic et al.*, 2010]. We document the tectonometamorphic evolution of tectonic units within the Sava Zone from continent-continent collision at the end of the Cretaceous to dominantly extensional tectonics associated with the formation of the Pannonian basin in the Neogene. P-T estimates and geochronological data from the metamorphics constrain the amount of tectonic overburden and the timing of the continent-continent collision. Our study also identifies for the first time a major detachment, responsible for the Oligocene to Miocene extensional unroofing of greenschist- to amphibolite-grade units in the internal Dinarides at the southern margin of the Pannonian basin.

1.2. Timing of Meliata-Vardar Ocean Closure

[5] A pertinent point for the argumentation developed in our study is that the final closure of the Meliata-Vardar Ocean postdates latest Jurassic to earliest Cretaceous ophiolite obduction. A remnant of the Meliata-Vardar Ocean remained open during the Cretaceous, as inferred from the following observations.

[6] 1. Metabasalts and glaucophane blueschists in Fruška Gora (part of the Sava Zone north of Beograd) yielding K-Ar ages of 123 ± 5 Ma on glaucophane [*Milovanović et al.*, 1995] suggest that subduction of remaining Vardar oceanic lithosphere underneath Europe-derived units was ongoing during the late Early Cretaceous.

[7] 2. Intraoceanic magmatism and pelagic sedimentation onto oceanic crust in the Sava Zone of North Bosnia indicate that a deep-marine seaway persisted at least until the Campanian [*Karamata et al.*, 2000, 2005; *Grubić et al.*, 2009; *Ustaszewski et al.*, 2009; *Vishnevskaya et al.*, 2009].

[8] 3. Late Cretaceous intrusives, volcanics and associated volcanosedimentary basins, stretching from southeast Bulgaria across Serbia into western Romania, informally referred to as "banatites" [*von Cotta*, 1864] or "Banat-Srednogorje Zone" [*Berza et al.*, 1998], show calc-alkaline affinity and span an age range from 93 to 72 Ma (early Turonian to late Campanian [*Nicolescu et al.*, 1999; *Georgiev et al.*, 2001; *Ciobanu et al.*, 2002; *Heinrich and Neubauer*, 2002; *Neubauer et al.*, 2003; *Handler et al.*, 2004; *von Quadt et al.*, 2005; *Rieser et al.*, 2008; *Zimmerman et al.*, 2008]), possibly as young as 66 Ma based on earlier K-Ar ages [*Neubauer*, 2002, and references therein]. Most authors interpret this association to have formed in an Andean arc or back-arc setting related to the north to NE directed subduction of the Meliata-Vardar branch of Neotethys beneath Europe-derived units [e.g., *Boccaletti et al.*, 1974; *Berza et al.*, 1998; *Ciobanu et al.*, 2002; *Neubauer*, 2002]. Subduction-related, bimodal volcanics of Late Cretaceous to earliest Paleocene age (110 to 62 Ma [*Pamić*, 1993b, 1997; *Pamić and Pécskay*, 1994; *Pamić et al.*, 2000]) are also known from sporadic exposures in the Croatian part of the Tisza-Dacia Mega-unit as well as from numerous boreholes in the Pannonian basin. It has been suggested that they are also part of the banatite belt [*Pamić*, 1998; *Pamić et al.*, 2000].

[9] 4. In central and south Serbia, the stratigraphic minimum age of strongly deformed, low-grade metamorphosed sediments of the Sava Zone, including olistoliths of mafics and ultramafics, as well as tectonically incorporated Mesozoic platform carbonates, is Late Cretaceous ("Senonian" flysch of *Dimitrijević* [1997, 2001], *Pamić* [2002], and *Schefer et al.* [2007]). Maastrichtian turbiditic sandstones containing olistoliths of blueschists [*Majer and Lugović*, 1991] also occur in the northern part of the Sava Zone in northern Bosnia (Figure 2) [*Jelaska et al.*, 1976; *Šparica et al.*, 1980; *Jelaska*, 1981; *Šparica et al.*, 1984; *Jovanović and Magaš*, 1986] and were interpreted as a synorogenic trench fill that was incorporated into an accretionary wedge [*Pamić*, 1993a].

[10] In the following, we attempt to better constrain the exact timing of the P-T-d path of such Late Cretaceous sediments that, following the collision between Adria and Europe, were overprinted by greenschist- to amphibolite-grade metamorphism (Figure 2) [*Pamić and Prohić*, 1989; *Pamić*, 1993a, 2002], and exhumed in the Neogene.

2. Regional Geological Setting

2.1. Sava Zone Suture

[11] Between the Aegean Sea and Beograd the Sava Zone suture is represented only by a NNW trending, a few kilometers wide belt of Late Cretaceous (Senonian) flysch (Figure 1). Near Beograd, the suture bends into an E-W trend and opens into an up to 50 km wide corridor of Late Cretaceous ophiolite-bearing units, trench sediments, magmatic rocks and metamorphic rocks running parallel to the Sava River (Figure 1). Between Beograd and Zagreb, these pre-Neogene rocks of the Sava Zone are only exposed in a few isolated inselbergs surrounded by Neogene sediments (Figure 2). The same applies to the Tisza-Dacia Mega-unit outcropping in the isolated Papuk-Psunj inselberg (Figures 2 and 3). The latter exposes pre-Mesozoic basement that experienced a pre-Variscan and syn-Variscan metamorphic overprint [*Pamić et al.*, 1988; *Pamić*, 2000; *Balen et al.*, 2006], and its low-grade metamorphic Permo-Mesozoic cover [*Biševac et al.*, 2009] (Figure 3). The northern edge of Papuk-Psunj hosts a small bimodal Late Cretaceous subvolcanic body that intruded the pre-Mesozoic basement [*Pamić*, 1997, 1998; *Pamić and Pécskay*, 1994]. Late Cretaceous bimodal volcanics are also known from boreholes in the vicinity of the Papuk-Psunj inselberg [*Pamić*, 1997] (Figure 3).

[12] The partly metamorphosed Late Cretaceous magmatic and sedimentary successions within the Sava Zone are unconformably overlain by Paleogene sediments [*Ustaszewski et al.*, 2009] (Figure 3). A correlation of the premetamorphic and postmetamorphic stratigraphic successions exposed in different inselbergs is provided in Figure 4. Only a few age assignments of stratigraphic intervals rely on the available biostratigraphic data (see Data Set S1).[1] Often the metamorphic overprint of the magmatic and sedimentary successions only allowed lithostratigraphic correlations.

2.2. Previous Data on Inselbergs at the Southern Rim of the Pannonian Basin

[13] Below we briefly review available data on the inselbergs that expose pre-Neogene rocks belonging to the Sava Zone and adjacent units between Zagreb and Beograd.

2.2.1. Moslavačka Gora

[14] Moslavačka Gora (Figures 2 and 3) exposes a crystalline basement characterized by Late Cretaceous LP-HT metamorphism and migmatization. The peak P-T conditions for this LP-HT metamorphic event were estimated at 550°C–660°C and 1.8–2.5 kbar [*Balen and Pamić*, 2000], perhaps reaching ~750°C and 3–4 kbar [*Starijaš et al.*, 2006, 2010]. The LP-HT metamorphosed metapelites and migmatites yielded electron-microprobe-based ("chemical") Th-U-Pb monazite ages between 100 and 90 Ma [*Starijaš et al.*, 2010]. The central S-type granite was dated at 82 ± 1 Ma by LA-

[1] Auxiliary material data sets are available at ftp://ftp.agu.org/apend/tc/2010tc002668. Other auxiliary material files are in the HTML.

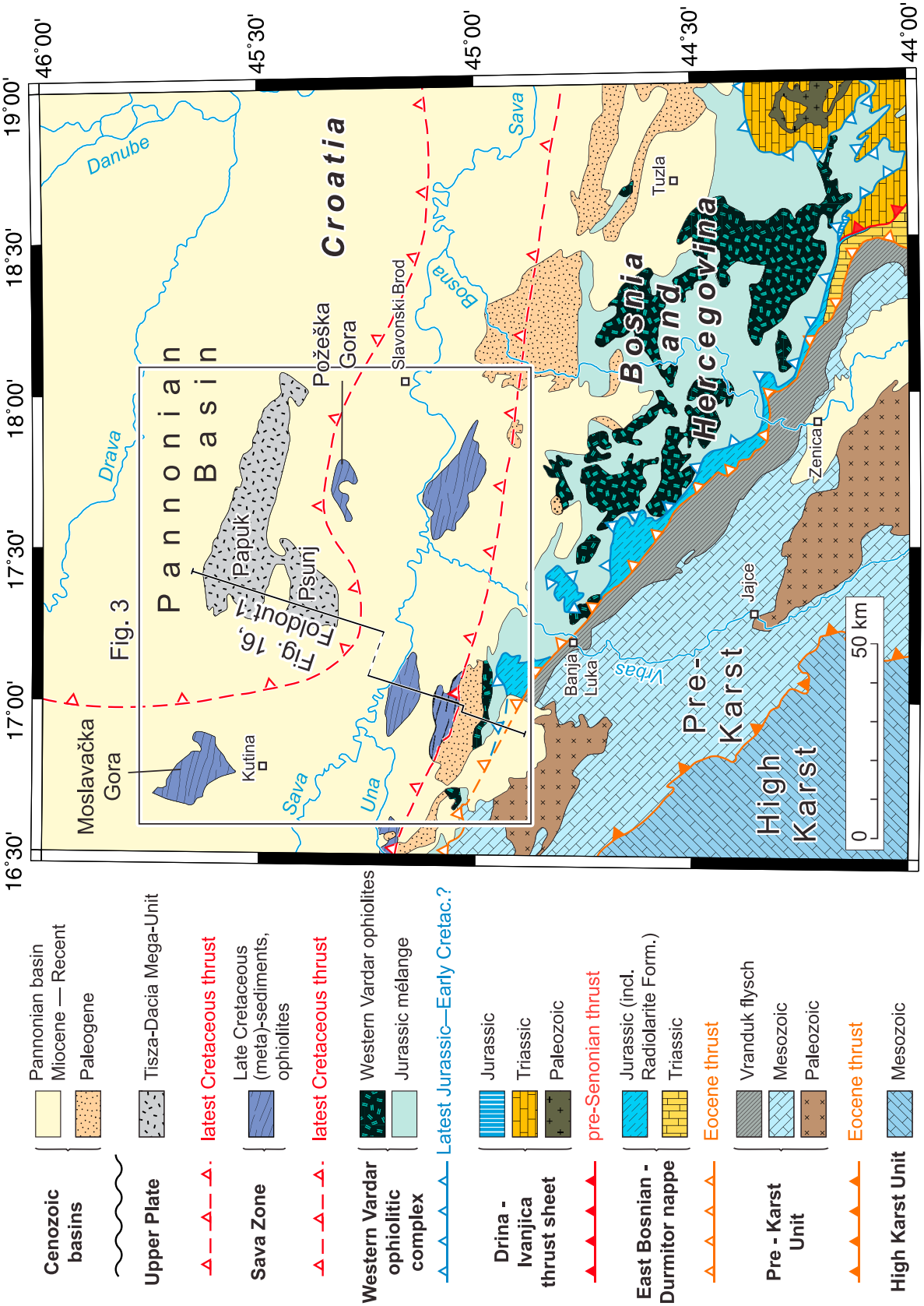

Figure 2. Tectonic map of the northern internal Dinarides and the northerly adjacent, Europe-derived Tisza-Dacia Mega-unit, separated by the Sava Zone suture.

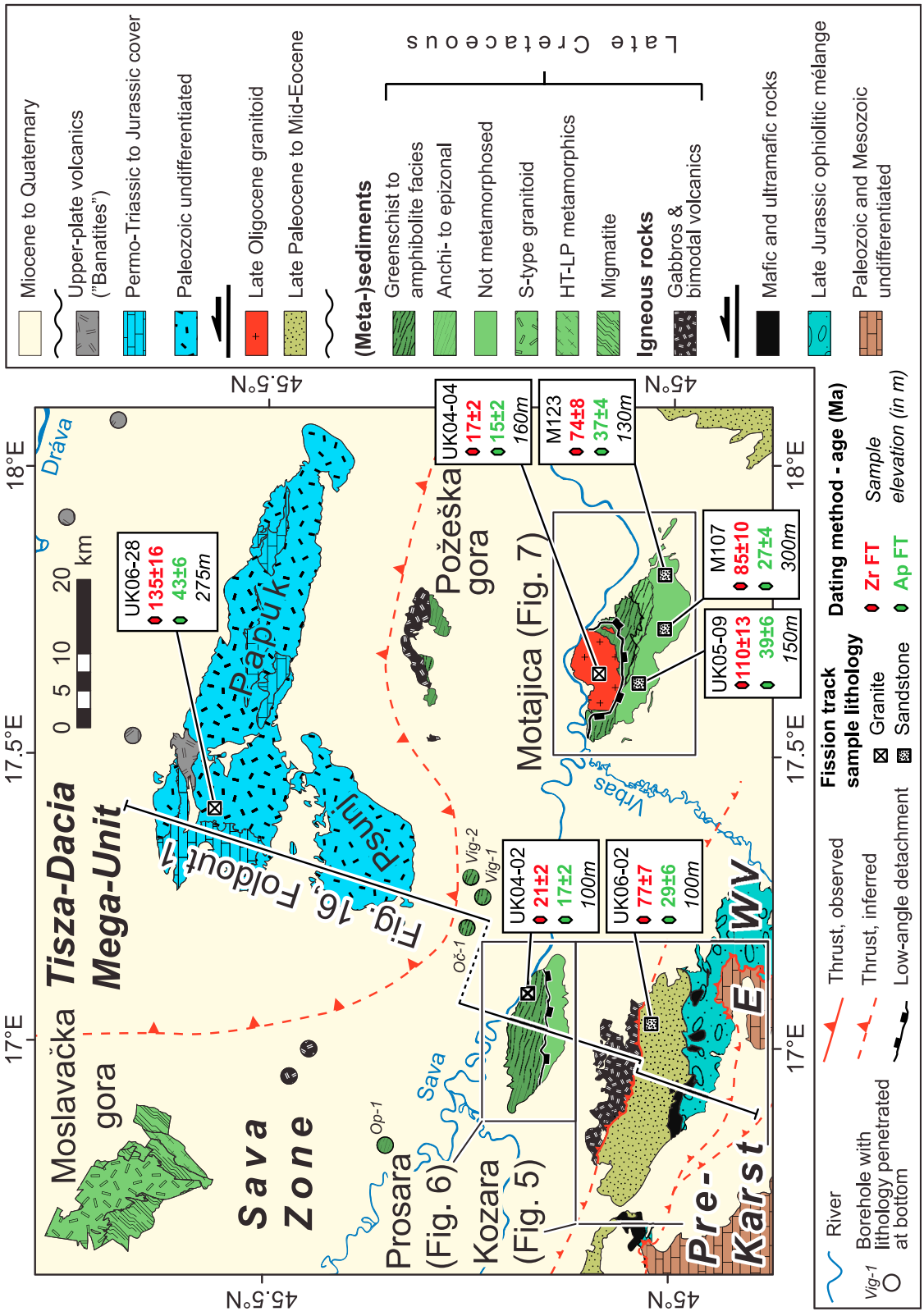

Figure 3. Simplified geologic-tectonic map of the study area, compiled from 1:100,000 map sheets of former Yugoslavia (referenced in the text) and *Pamić et al.* [2000]. Well locations are from *Lamphere and Pamić* [1992] and *Pamić* [1997]. Selected fission track results illustrate the contrasting Neogene thermal evolution of the Sava Zone metamorphics with respect to adjacent tectonic units. Some fission track results from the Kozara and Motajica inselbergs were omitted for the sake of legibility; the complete data sets are shown in Figures 5 and 7. E, East Bosnian–Durmitor nappe; WV, western Vardar Ophiolite Complex.

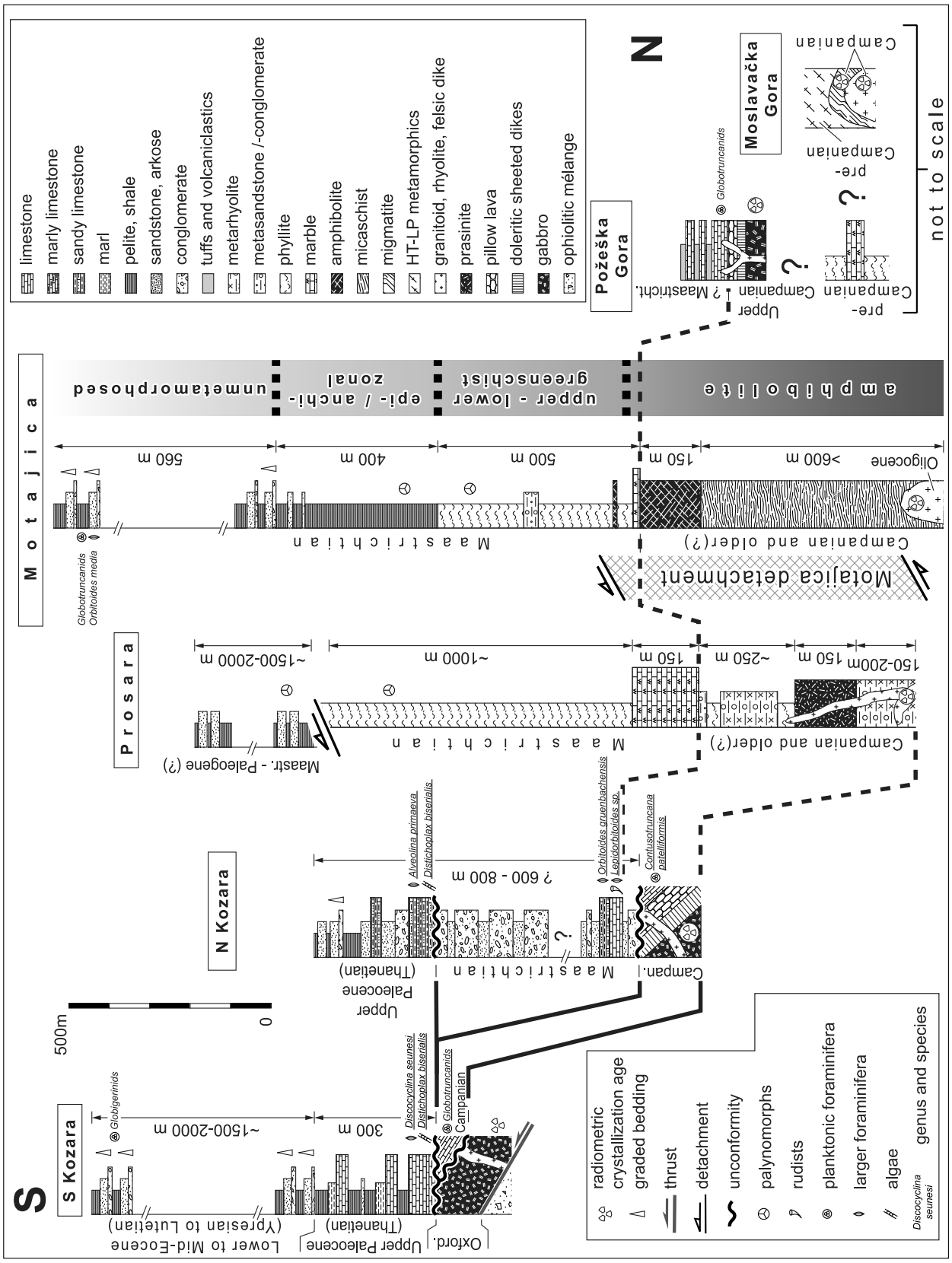
S
S Kozara
500m
0
~1500-2000 m
300 m
Globigerinids
Discocyclina seunesi
Globotruncanids
Campanian
Oxford.
Upper Paleocene (Thanetian)
Lower to Mid-Eocene (Ypresian to Lutetian)
N Kozara
? 600 - 800 m
Alveolina primaeva
Distichoplax biserialis
Orbitoides gruenbachensis
Lepidorbitoides sp.
Contusotruncana patelliformis
Campan.
M a a s t r i c h t i a n
Upper Paleocene (Thanetian)
Prosara
Maastr. - Paleogene (?)
~1500-2000 m
~1000 m
150 m
~250 m
150-200m
Globotruncanids
Orbitoides media
Motajica
M a a s t r i c h t i a n
Campanian and older(?)
560 m
400 m
500 m
150 m
>600 m
Oligocene
unmetamorphosed
epi- / anchi- zonal
upper - lower greenschist
amphibolite
Motajica detachment
limestone
marly limestone
sandy limestone
marl
pelite, shale
sandstone, arkose
conglomerate
tuffs and volcaniclastics
metarhyolite
metasandstone /-conglomerate
phyllite
marble
amphibolite
micaschist
migmatite
HT-LP metamorphics
granitoid, rhyolite, felsic dike
prasinite
pillow lava
doleritic sheeted dikes
gabbro
ophiolitic mélange
Požeška Gora
Upper Campanian ? Maastricht.
pre-Campanian
Globotruncanids
Moslavačka Gora
pre-Campanian
Campanian
N
not to scale
radiometric crystallization age
graded bedding
thrust
detachment
unconformity
palynomorphs
rudists
planktonic foraminifera
larger foraminifera
algae
Discocyclina seunesi
genus and species

Figure 4

ICP-MS zircon dating [*Starijaš et al.*, 2010]. $^{40}Ar/^{39}Ar$ ages on hornblende and white mica document cooling from peak metamorphic conditions between 83 and 74 Ma [*Balen et al.*, 2001]. As yet, this early Late Cretaceous metamorphic event was not identified elsewhere within the Sava Zone and its geodynamic significance remains enigmatic.

2.2.2. Požeška Gora

[15] The northern part of Požeška Gora (Figures 2 and 3) exposes a bimodal igneous rock suite including (gabbro-) dolerites, pillow basalts, basic and acidic tuffs and volcaniclastics, as well as alkali-feldspar rhyolites and volumetrically subordinate granites [*Pamić and Šparica*, 1983; *Šparica and Pamić*, 1986; *Belak et al.*, 1998]. Pillow basalts and tuffs are interbedded with fossiliferous red, pelagic limestones that yielded Late Campanian to Early Maastrichtian globotruncanids [*Pamić and Šparica*, 1983; *Jamičić*, 2007; M. Caron, personal communication, 2007]. Dolerite dikes intrude both acidic rocks and the Late Cretaceous pelagic sediments [*Belak et al.*, 1998]. Rhyolites and cogenetic granites gave a Rb-Sr age of 71.5 ± 2.8 Ma [*Pamić et al.*, 1988]; K-Ar ages of the dolerites range between 68 and 66 Ma [*Pamić*, 1993b].

[16] The southern part of Požeška Gora hosts exposures of greenschist facies phyllites, quartz-muscovite schists, greenschists and calcite marbles [*Šparica and Pamić*, 1986; *Pamić*, 1998]. K-Ar whole rock ages obtained on quartz-muscovite phyllites yielded an age of ~49 Ma [*Pamić et al.*, 1988], which may indicate the timing of or cooling from peak metamorphic conditions. Due to poor outcrop conditions, the structural relationships between the Late Cretaceous volcanic/volcanoclastic succession and the metamorphics are unknown as yet [see *Šparica et al.*, 1980; *Šparica and Pamić*, 1986].

2.2.3. Kozara

[17] Kozara Mountain includes two tectonically juxtaposed ophiolitic successions of different age, separated by a belt of Paleogene sediments (Figures 3 and 5). South Kozara Mountain exposes obducted western Vardar ophiolites of Jurassic age, whereas North Kozara Mountain exposes a Late Cretaceous igneous and sedimentary succession of oceanic origin [*Ustaszewski et al.*, 2009]. The western Vardar ophiolites of South Kozara are unconformably overlain by Late Paleocene (Thanetian) shallow-water limestones (Figures 4 and 5) that grade upsection into Early to Middle Eocene (Ypresian to Lutetian) turbiditic sandstones [*Blanchet*, 1970; *Šparica et al.*, 1984; *Jelaska*, 1981; *Jovanović and Magaš*, 1986; *Ustaszewski et al.*, 2009]. This unconformable succession on top of the western Vardar ophiolites was either interpreted as a postcollisional molasse succession [*Aubouin et al.*, 1970; *Jelaska et al.*, 1970], or alternatively, as a flysch succession ("Kozara Flysch" [*Šparica et al.*, 1984; *Jovanović and Magaš*, 1986]). The intraoceanic igneous succession of North Kozara is thrust onto these Paleogene sediments (Figures 3 and 5). This bimodal igneous succession comprises isotropic gabbros, doleritic dikes, basaltic pillow lavas and rhyolites (Figure 5). Pelagic limestones, intercalated with the pillow lavas, yield Campanian globotruncanids [*Grubić et al.*, 2009; *Ustaszewski et al.*, 2009] and radiolarians [*Vishnevskaya et al.*, 2009], which is consistent with concordant U-Pb ages (81–82 Ma) on zircons derived from dolerites and rhyolites [*Ustaszewski et al.*, 2009].

2.2.4. Prosara

[18] Prosara Mountain exposes two contrasting units (Figures 3 and 6a). A nonmetamorphic succession of shales and sandstones of Maastrichtian to possibly Paleogene age [*Šparica et al.*, 1984; *Jovanović and Magaš*, 1986] (see Figure 4 and Data Set S1) in the south is fault bounded against a greenschist facies metasedimentary, subordinately metavolcanic succession to the north. Palynomorphs preserved in metamorphic phyllites, the most common lithology in the north, suggested a Maastrichtian [*Šparica et al.*, 1984] (see Data Set S1) or generally Late Cretaceous [*Jovanović and Magaš*, 1986] depositional age.

2.2.5. Motajica

[19] Motajica inselberg exposes a dominantly siliciclastic succession of Late Cretaceous (Maastrichtian and probably older) age [*Pantić and Jovanović*, 1970; *Šparica et al.*, 1980] (Figures 3 and 7). This succession is lithologically similar to the metamorphosed successions from Prosara and Požeška Gora. The structurally lower parts exposed in the north underwent Barrovian metamorphism reaching amphibolite grade [*Pamić and Prohić*, 1989; *Pamić et al.*, 1992; *Pamić*, 1998]. Chemical Th-U-Pb monazite ages (63 ± 9 Ma) suggest a latest Cretaceous to early Paleogene age for this metamorphic event [*Krenn et al.*, 2008]. A granitoid pluton encompassing two-mica granites, granodiorites, monzogranites, monzodiorites, as well as subordinate quartz diorites and leucogranites [*Varičak*, 1966; *Pamić and Prohić*, 1989; *Jurković*, 2004] intrudes the metamorphics. Based on major and trace element geochemistry as well as Sr-isotopic data, the granitoids were first considered as S-type [*Pamić and Prohić*, 1989] and later, with a larger data set, as transitional between S- and I-type [*Pamić and Balen*, 2001; *Pamić et al.*, 2002]. Whole rock Rb-Sr dating of three granitic samples suggest an age of intrusion at 48.7 ± 1.5 Ma [*Lanphere and Pamić*, 1992], the younger biotite K-Ar age of 18.1 Ma may represent a cooling age [*Lanphere and Pamić*, 1992].

2.2.6. Cer

[20] Although this inselberg in western Serbia (Figure 8) is part of the Jadar-Kopaonik thrust sheet, i.e., structurally in a more external position in respect to the Sava Zone [*Schmid et al.*, 2008], it shares many structural similarities with Motajica inselberg. Granitoids encompassing leucocratic and muscovite granites, quartz monzonites, granodiorites and

Figure 4. Tectonostratigraphic correlation of the successions exposed in the Sava Zone inselbergs (see Figures 2 and 3 for location). Solid thick lines mark correlated stratigraphic intervals and unconformities with biostratigraphic control (see Data Set S1). Dashed thick lines mark lithostratigraphically correlated horizons. Underlined fossils are from *Ustaszewski et al.* [2009], and all other fossils are from older sources [*Jovanović and Magaš*, 1986; *Pamić and Šparica*, 1983; *Pantić and Jovanović*, 1970; *Šparica et al.*, 1980, 1984]. The metamorphic grade of metasediments in Motajica is indicated.

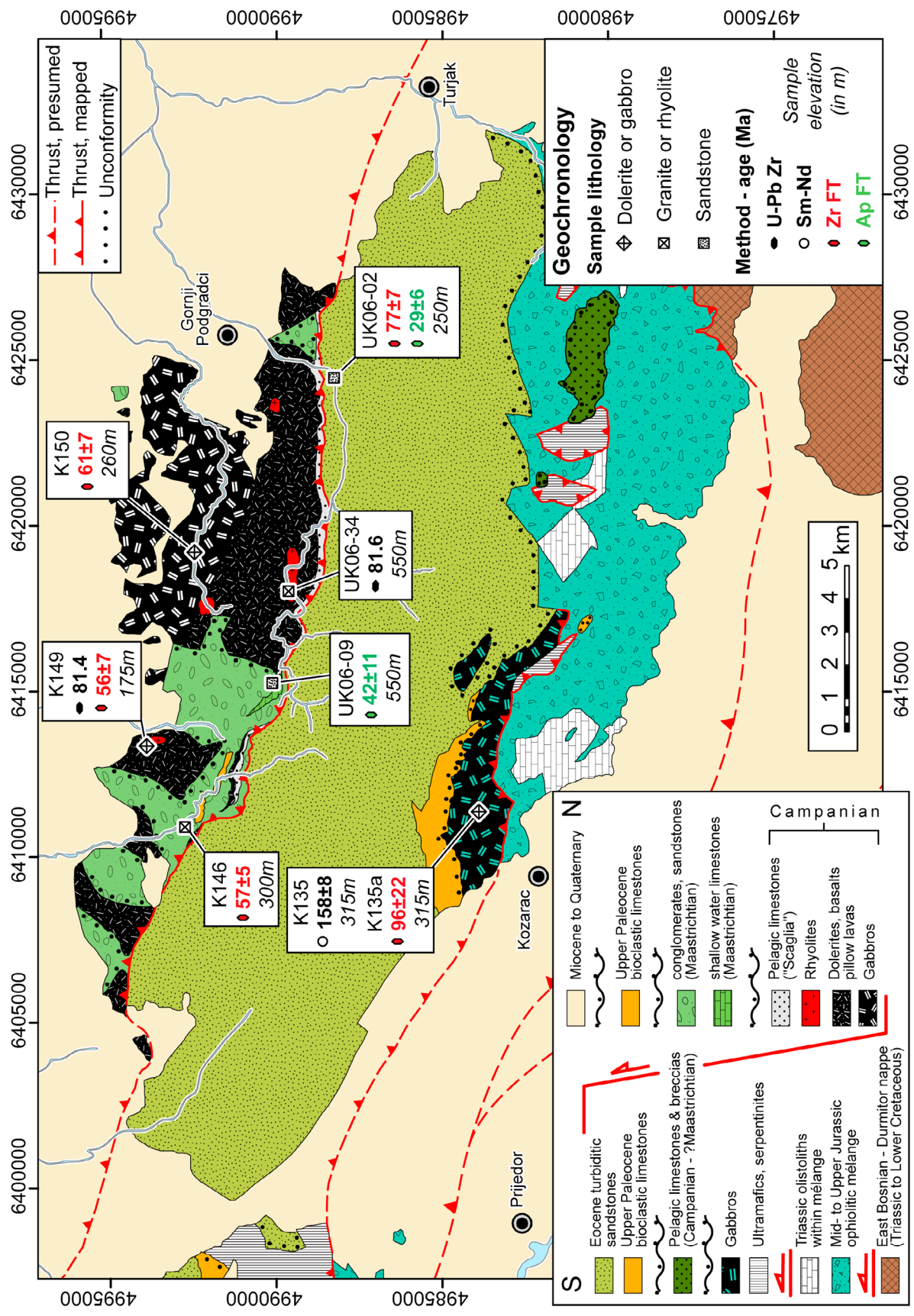

Figure 5. Geological map of the Kozara inselberg. Numbers at the edges of this map and Figures 6–8 are MGI Balkan Zone 6 Cartesian coordinates. U-Pb and Sm-Nd ages are from *Ustaszewski et al.* [2009].

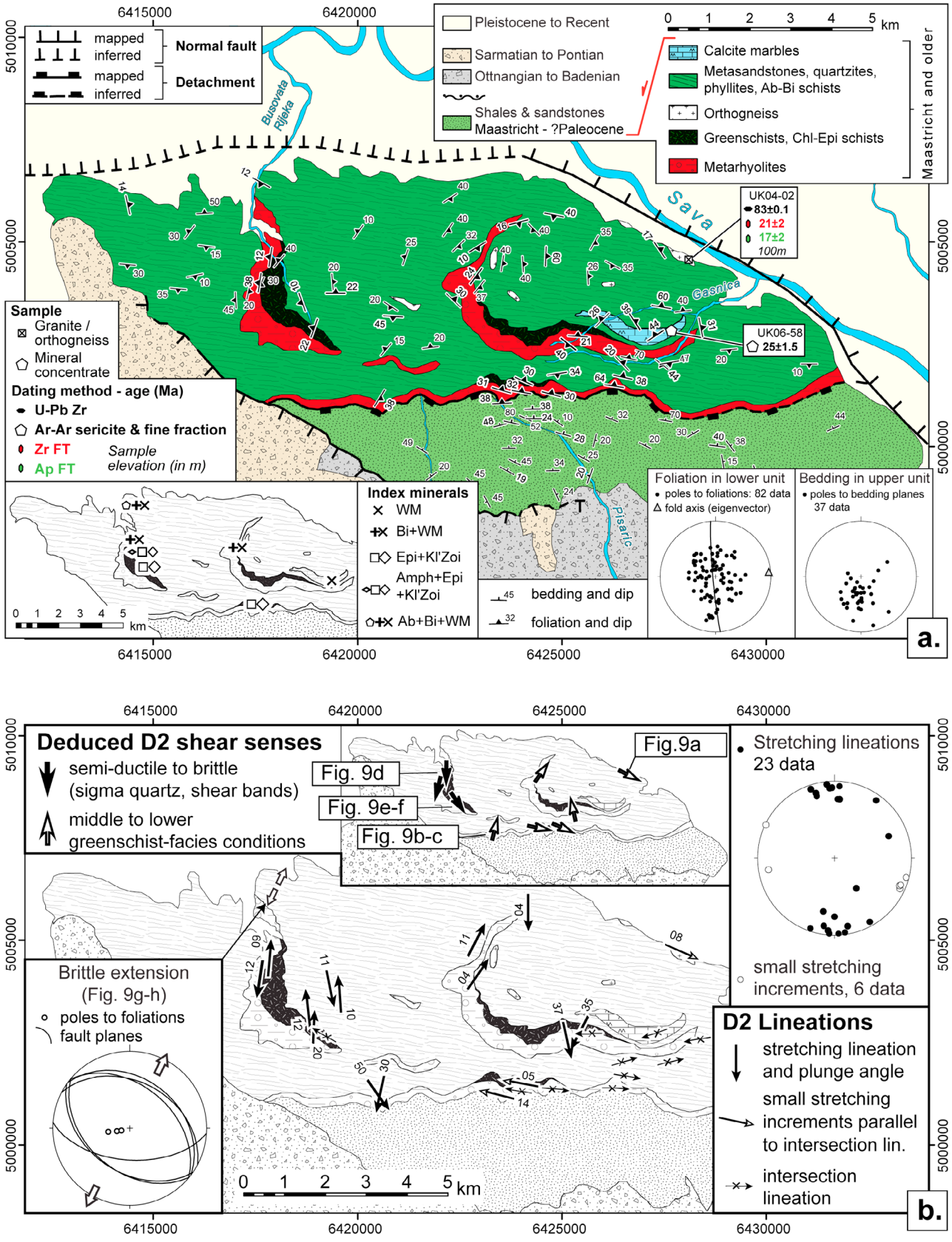
6415000
6420000
6425000
6430000
5010000
5005000
5000000
mapped
inferred
Normal fault
mapped
inferred
Detachment
Pleistocene to Recent
Sarmatian to Pontian
Ottnangian to Badenian
Shales & sandstones
Maastricht - ?Paleocene
0 1 2 3 4 5 km
Calcite marbles
Metasandstones, quartzites, phyllites, Ab-Bi schists
Orthogneiss
Greenschists, Chl-Epi schists
Metarhyolites
Maastricht and older
Buzovata Rijeka
Sava
Gasnica
Pisarić
UK04-02
83±0.1
21±2
17±2
100m
UK06-58
25±1.5
Sample
Granite / orthogneiss
Mineral concentrate
Dating method - age (Ma)
U-Pb Zr
Ar-Ar sericite & fine fraction
Zr FT
Ap FT
Sample elevation (in m)
Index minerals
WM
Bi+WM
Epi+Kl'Zoi
Amph+Epi +Kl'Zoi
Ab+Bi+WM
bedding and dip
foliation and dip
Foliation in lower unit
poles to foliations: 82 data
fold axis (eigenvector)
Bedding in upper unit
poles to bedding planes
37 data
a.
Deduced D2 shear senses
semi-ductile to brittle
(sigma quartz, shear bands)
middle to lower
greenschist-facies conditions
Fig. 9d
Fig. 9e-f
Fig. 9b-c
Fig.9a
Stretching lineations
23 data
small stretching
increments, 6 data
Brittle extension
(Fig. 9g-h)
poles to foliations
fault planes
D2 Lineations
stretching lineation
and plunge angle
small stretching
increments parallel
to intersection lin.
intersection
lineation
b.

Figure 6

subordinate two-mica granites [*Knežević*, 1962; *Knežević et al.*, 1994a, 1994b; *Koroneos et al.*, 2010] intrude low-grade Paleozoic and Mesozoic sediments that are part of the footwall of the obducted western Vardar ophiolites. Foliation and bedding in the country rocks wrapped around the pluton are concordant to a magmatic foliation developed in the outer parts of the intrusion. Available radiometric data show a large spread: hornblende and whole rock K-Ar ages range between 30 and 22 Ma, while K-Ar ages of muscovite and biotite range between 18 and 15 Ma [*Knežević et al.*, 1994b]. *Koroneos et al.* [2010] interpret the Cer pluton as a multiphase intrusion, in which metaluminous I-type quartz monzonites and monzodiorites are intruded by peraluminous S-type two-mica granites. According to them, K-Ar dating suggests that the I-type magmatics were emplaced not later than at 21 Ma, while the S-type granitoids are as young as 19 to 16 Ma.

3. New Data on the Structural and Metamorphic Evolution of the Prosara and Motajica Inselbergs

3.1. Prosara Inselberg

[21] The middle to upper greenschist facies succession exposed in the northern part of Prosara comprises metarhyolites, epidote-amphibole greenschists derived from mafic intrusions, chlorite-epidote schists, albite-biotite schists, metasandstones, phyllites and subordinate orthogneisses and calcite marbles (Figure 6a); Mineral assemblages identified are shown in the bottom left inset of Figure 6a. Metarhyolites and associated greenschists occur in two different structural levels. Small occurrences of coarse-grained, leucocratic granites show a gneissic schistosity that is concordant with that of the surrounding phyllites (orthogneisses of Figure 6a). The following observations indicate low-grade solid-state deformation of these granitoids: (1) feldspar porphyroclasts show undulatory extinction, bookshelf deformation and fracturing (Figure 9a); they broke down to epidote and zoisite/clinozoisite; (2) magmatic white mica largely recrystallized to fine-grained sericite (Figure 9a); and (3) quartz forms elongated aggregates parallel to the foliation and shows bulging recrystallization [*Stipp et al.*, 2002].

[22] This succession is fault bounded against the northerly adjacent Neogene basin, as well as against southerly adjacent nonmetamorphic Late Cretaceous sediments (Figure 6a). The northern fault is partly covered by Pleistocene to recent colluvial deposits. Bedding in the southerly adjacent nonmetamorphosed sediments dominantly dips north. The structure of the greenschist facies unit is characterized by an E-W trending synform defined by the dip of the dominant foliation (Figure 6a). At a few locations the dominant foliation was found to overprint an earlier foliation; corresponding intersection lineations trend roughly E-W (Figure 6b). Owing to this outcrop-scale observation, we term the earlier foliation s1 and the dominant foliation s2. Deformation associated with s2 led to mylonitization within those levels containing metarhyolites and metasandstones. Moderately plunging L2 stretching lineations contained in s2 trend approximately N-S (Figure 6b). Shear senses associated with L2 indicate both top-to-the-north and top-to-the-south shearing (Figures 6b and 9b). Top-to-the-north shear senses are associated with a pronounced shape-preferred orientation of quartz aggregates and are characterized by grain boundary bulging and beginning of subgrain rotation recrystallization [*Stipp et al.*, 2002], which suggests deformation at temperatures around 350°C to 450°C during D2 (Figures 9b and 9c). We also observed subordinate ductile shear parallel to E-W trending s1–s2 intersection lineations, indicating small increments of trend-parallel, top-to-the-east directed sense of shear (Figure 6b), suggesting that extension was probably multidirectional.

[23] Later increments of D2 shearing associated with L2 are inferred to have occurred under decreasing temperatures (Figures 9d–9h). In contrast to the aforementioned, "early" D2 shear senses, they all indicate top-to-the-south shear. Top-to-the-south semiductile extensional shear bands (Figures 9e and 9f) and brittle conjugate faults dissecting the metamorphic foliation (Figures 9g and 9h) suggest that N-S directed D2 extension affected the metamorphic succession all the way into the brittle regime.

[24] In summary, the metamorphic succession of Prosara underwent progressive cooling and exhumation from about midgreenschist facies to brittle conditions associated with N-S extension during D2. Fission track dating, presented in section 4.3, indicates that this extension is related to the early Miocene rifting phase of the Pannonian basin.

3.2. Motajica Inselberg

[25] The new structural and petrographic observations below start with the structurally highest units exposed in the south and progress downsection toward north.

3.2.1. Low-Grade Shales and Sandstones

[26] South dipping low-grade shales and moderately to well-sorted sandstones make up the southern half of Motajica inselberg (Figure 7a). No newly grown minerals are visible in thin section. Illite crystallinity (IC) was determined in selected low-grade shales (Figure 7b). The minerals, determined by XRD, include quartz, calcite, chlorite, muscovite and feldspar. Analyses of the <0.25 μm fraction yielded a Kübler index (KI) of 0.33 after standardization, indicating low anchizonal conditions [*Kisch*, 1990, 1991; *Warr and Rice*, 1994]. Additionally, the measured ÁI value of 0.29 (ÁI = Árkai

Figure 6. (a) Geological map of the Prosara inselberg, compiled from 1:100,000-scale geological map sheets of former Yugoslavia [*Šparica et al.*, 1984; *Jovanović and Magaš*, 1986] and modified according to our own observations. Bottom left inset shows selected newly formed metamorphic index minerals and parageneses identified in thin sections in the lower tectonic unit. Mineral abbreviations are as follows: Ab, albite; Amph, amphibole; Bi, biotite; Epi, epidote; Kl'Zoi, clinozoisite; WM, white mica. See Figure 3 for location. (b) Lineations and shear sense indicators observed in the lower tectonic unit. Extension is multidirectional. We observe a change in the sense of shear from top to the east and top to the north to top to the south with decreasing temperature of deformation. See also thin section and outcrop observations in Figure 9. Lithology patterns are identical to Figure 6a.

index or chlorite crystallinity [*Árkai et al.*, 1995; *Árkai and Sadek Ghabrial*, 1997]) again corresponds to anchizonal conditions (T ≈ 200°C–300°C). This confirms the previously obtained IC values for lithologically and structurally identical samples reported by *Pamić et al.* [1992].

3.2.2. Greenschist Facies Phyllites

[27] The phyllites structurally underlie the low-grade shales and sandstones. They represent a monotonous quartz-poor succession, lithologically comparable to the phyllites in Prosara. Prograde growth of chlorite, biotite and white mica indicates that mid to upper greenschist facies conditions were reached (Figure 7b). The presence of epidote and zoisite/clinozoisite, also indicative of mid to upper greenschist facies conditions, is restricted to the structurally lowermost parts of this succession (Figure 7b).

3.2.3. Amphibolite Facies Lithologies and Mineral Assemblages

[28] Amphibolite facies lithologies include amphibolites, metapelites and subordinate paragneisses. Amphibolites contain green, tschermakitic amphibole, some clinozoisite, epidote and subordinate biotite. The metapelites are mostly staurolite- and/or garnet-bearing micaschists. Staurolite, biotite, white mica, plagioclase and quartz (Figure 10a) form a common mineral assemblage; garnet and biotite are often in textural equilibrium. However, well-preserved mineral assemblages are the exception since numerous metapelite samples show widespread chloritization of garnet and biotite (Figure 10b).

3.2.4. Granitoid Pluton

[29] The pluton is texturally isotropic in the center but foliated along its margins (Figure 7a). In foliated granitoids quartz and feldspar show abundant undulatory extinction. Zoisite/clinozoisite and epidote, often in elongated bands parallel to the foliation, formed at the expense of magmatic K-feldspar and plagioclase (Figures 10c and 10d). The contact to the adjacent units is sharp and generally lacks a contact aureole. A rapid increase in the size of mica porphyroblasts is observed locally, where fine-grained greenschist facies phyllites are juxtaposed against the granitoid. This transition occurs within a distance of some 100–150 m. At one locality, andalusite and white mica porphyroblasts were observed in metapelites at the contact to the intrusion (Figure 7b). The andalusite forms pseudomorphs after fibrous sillimanite, suggesting that it postdates regional metamorphism.

3.2.5. Structures

[30] In the greenschist and amphibolite facies lithologies the main metamorphic foliation (s1) strikes approximately ENE-WSW and parallels the bedding in the overlying low-grade Maastrichtian sandstones and shales (Figure 7a). A mineral stretching lineation associated with s1 was observed in only one location. It is associated with quartz mylonites with a pronounced shape-preferred orientation and a top-to-the-SE directed sense of shear (Figures 10e and 10f). Both s1 foliation and L1 lineation are interpreted to be associated with a D1 deformation stage, related to the main metamorphic event.

[31] Overprinting of the s1 foliation by a younger foliation s2 was observed at the outcrop scale (Figures 10g and 10h), predominantly in the micaschists. Within the amphibolites and phyllites s2 was only observed in a few sites (Figure 7a). S1 becomes increasingly transposed by s2 in the vicinity of the intrusion. S2 strikes often at a high angle to s1, particularly along the western margin of the intrusion (Figure 7a), where s2 intersects s1 almost perpendicularly. We interpret this s2 foliation to be related to a second deformation phase D2, which postdates the granite intrusion. In areas where D2 strain is low, s2 developed a spaced axial plane cleavage. In the s2 axial planes of nonretrogressed micaschists the growth of a second generation of biotite (Figure 10i), indicates that D2 deformation must have initiated under at least mid-greenschist facies conditions. In the phyllites s2 mostly forms a crenulation cleavage (Figure 10j). In areas where D2 strain is high, s1 was totally overprinted.

[32] L2 stretching lineations associated with s2 generally trend WNW-ESE (Figure 7c). These are mainly observed in amphibolite facies metapelites and paragneisses, only rarely within the immediately adjacent phyllites, and entirely absent in higher and colder structural levels in the south (Figure 7c). The D2-related foliations and lineations hence define an up to 2 km wide zone of ductile deformation, comprising the periphery of the Motajica granite and its amphibolite-grade frame (Figure 7c). Within this zone of ductile D2 deformation, referred to as Motajica detachment, both top-to-the-west and top-to-the-east senses of shear are observed (bottom left inset in Figure 7c). High-temperature D2 microstructures (upper greenschist facies; Figures 10k and 10l) indicate a top-to-the-WNW tectonic transport, while shear senses related to deformation that occurred under decreasing temperatures (Figures 10m and 10n) point away from the intrusion (bottom left inset of Figure 7c). Extensional shear bands (Figure 10n) often contain chlorite that replaces biotite, directly evidencing widespread retrogression of mineral assemblages during D2 (Figure 10b).

[33] Interpretative geological sections across Motajica inselberg, based on both mesoscopic and microstructural observations, illustrate the large-scale structural context (Figure 11). Extensional faulting along the Motajica detach-

Figure 7. Geological map of the Motajica inselberg, compiled from 1:100,000-scale geological map sheets of former Yugoslavia [*Šparica et al.*, 1980] and modified according to our own observations. (a) Major lithological units, foliations, and faults. (b) Metamorphic index minerals identified in thin sections. Mineral abbreviations are as follows: And, andalusite; Bi, biotite; Chl, chlorite; Epi, epidote; Gar, garnet; Hbl, hornblende; Kl'Zoi, clinozoisite; Stau, staurolite; WM, white mica; Zoi, zoisite. White mica is ubiquitous in all occurrences of staurolite. (c) Map of mineral stretching lineations and deduced shear senses. The "Motajica detachment" was outlined based on the extent of s2 foliations (Figure 7a) and D2 stretching lineations. (d) Geochronological data in the Motajica inselberg. Underlined samples are those for which the confined track length distributions of apatites are shown in the bottom inset. The horizontal axis shows track lengths in microns, and the vertical axis shows the number of grains.

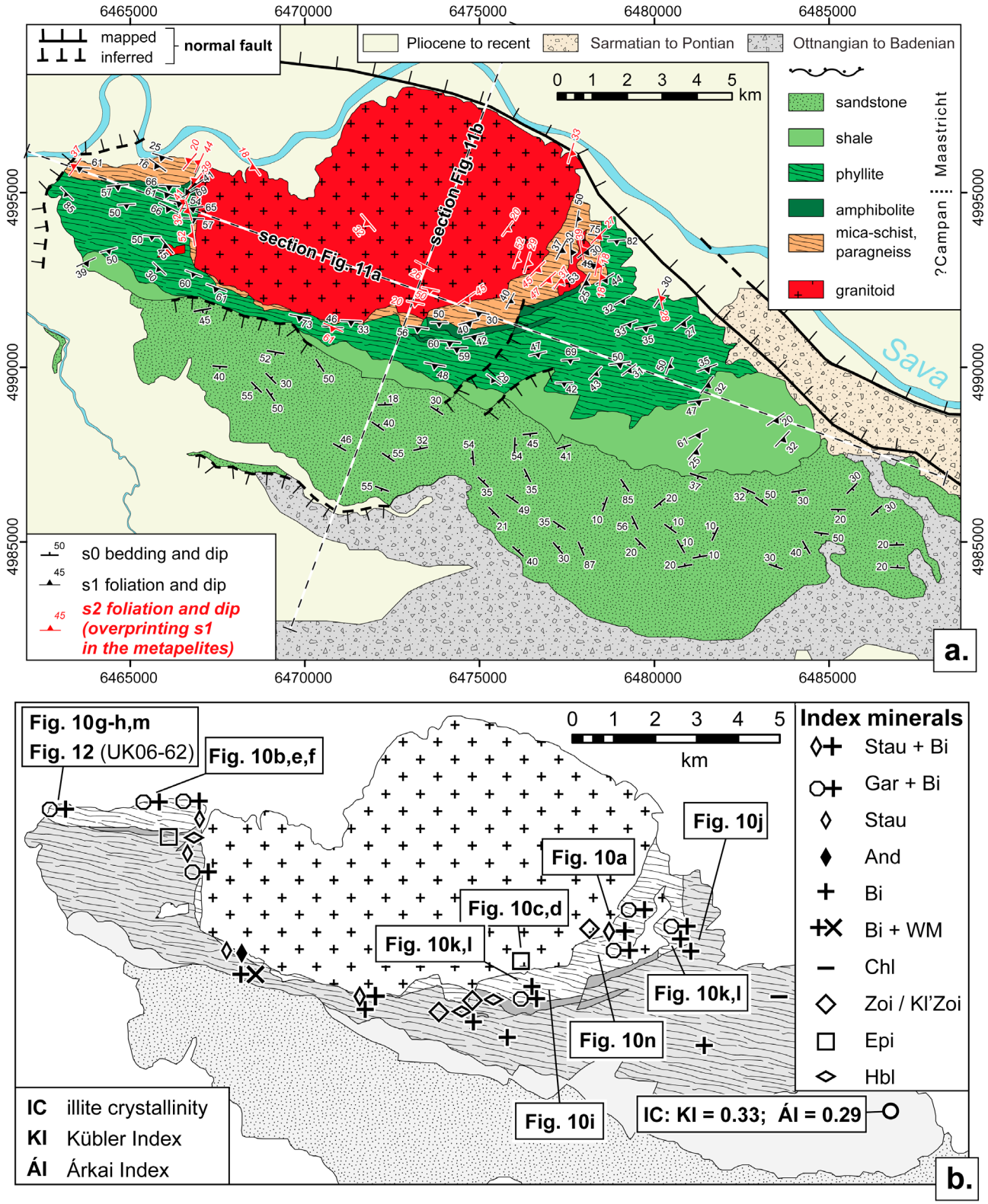
6465000
6470000
6475000
6480000
6485000
4995000
4990000
4985000
mapped
inferred
normal fault
Pliocene to recent
Sarmatian to Pontian
Ottnangian to Badenian
0 1 2 3 4 5
km
sandstone
shale
phyllite
amphibolite
mica-schist, paragneiss
granitoid
Maastricht
?Campan
Sava
section Fig. 11a
section Fig. 11b
s0 bedding and dip
s1 foliation and dip
s2 foliation and dip (overprinting s1 in the metapelites)
a.
Fig. 10g-h,m
Fig. 12 (UK06-62)
Fig. 10b,e,f
Fig. 10j
Fig. 10a
Fig. 10c,d
Fig. 10k,l
Fig. 10k,l
Fig. 10n
Fig. 10i
Index minerals
Stau + Bi
Gar + Bi
Stau
And
Bi
Bi + WM
Chl
Zoi / Kl'Zoi
Epi
Hbl
IC: Kl = 0.33; ÁI = 0.29
IC illite crystallinity
Kl Kübler Index
ÁI Árkai Index
b.

Figure 7

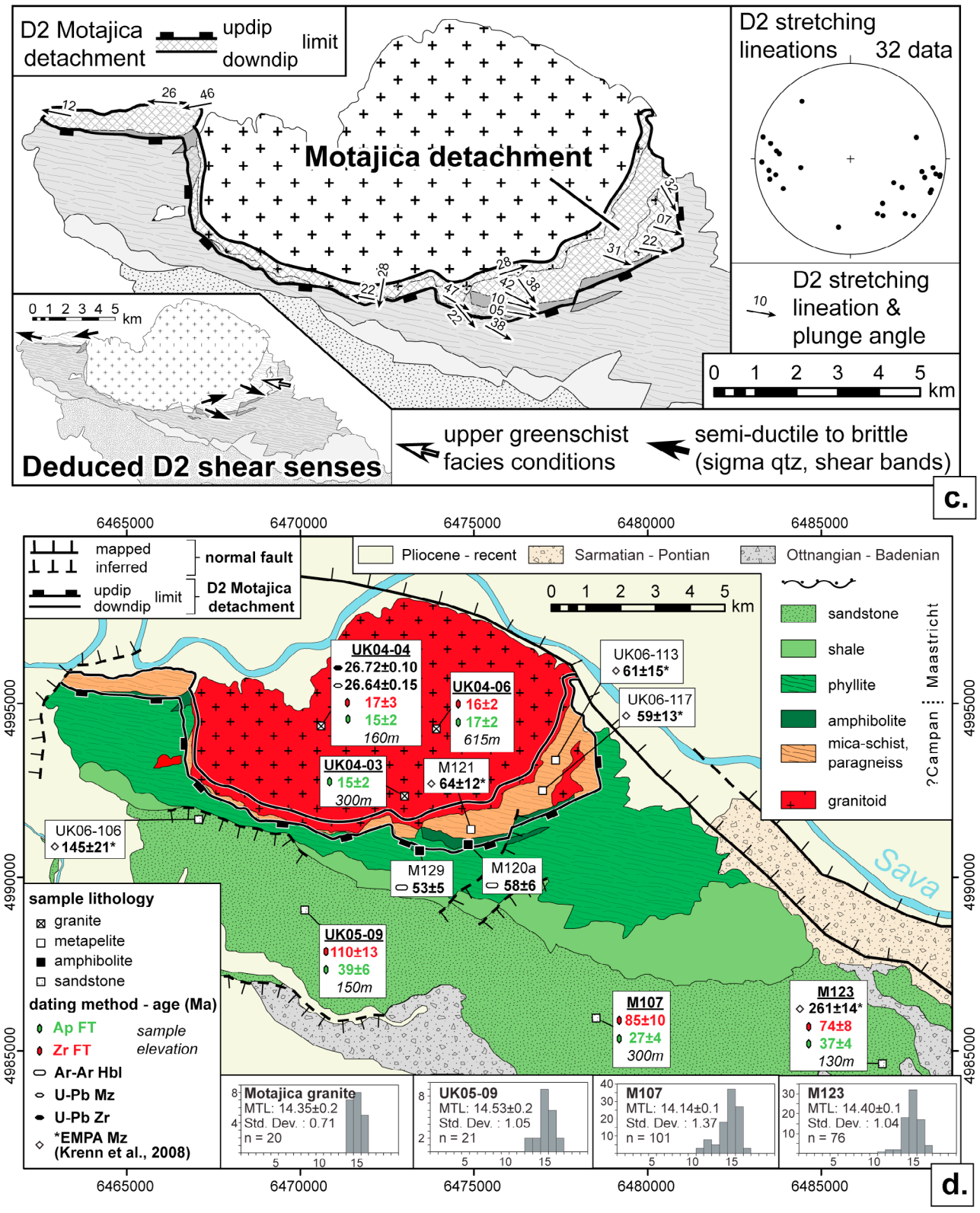

Figure 7. (continued)

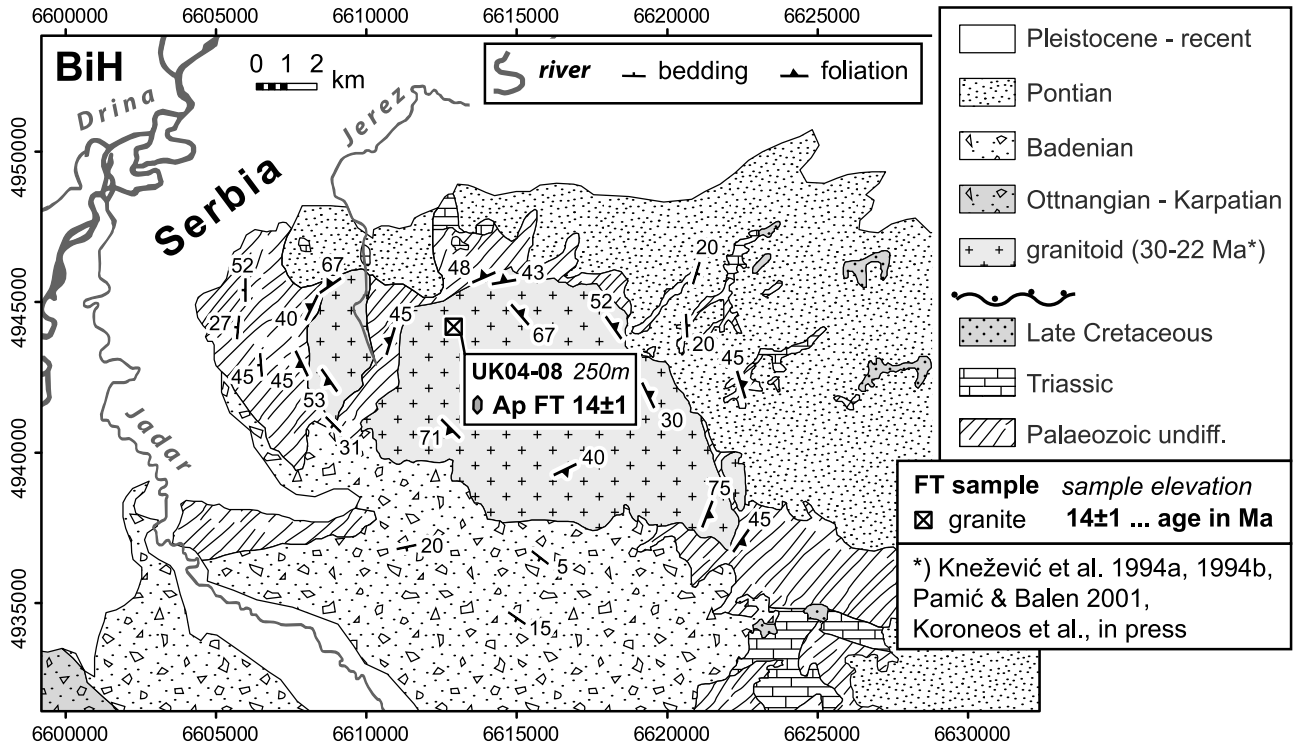

Figure 8. Tectonic map of Cer inselberg in western Serbia, compiled from 1:100,000-scale geological map sheets of former Yugoslavia [*Filipović et al.*, 1967; *Mojsilović et al.*, 1975] with location and age of an apatite fission track sample from this study. See Figure 1 for location of the map. BiH, Bosnia and Hercegovina.

ment during D2 (Figures 7c, 7d, and 11) leads to tectonic omission and a vertically telescoped field metamorphic gradient. This interpretation will be corroborated by fission track dating results presented later.

3.2.6. Pressure-Temperature Estimates of Amphibolite Facies Metamorphism During D1

[34] Peak pressure and temperature (PT) conditions reached during D1 were inferred from identification of equilibrium mineral assemblages, phase equilibrium modeling ("pseudosections") and thermobarometry. The composition of the major mineral phases was obtained using a JEOL JX8600 microprobe housed at Salzburg University (analysis routine of *Krenn and Finger* [2004] and *Gaidies et al.* [2008]). Whole rock analysis was performed by standard XRF methods with a Brucker S4 Pioneer WD spectrometer at Salzburg University. The mineral assemblage in the analyzed metapelites commonly is Grt, Pl, Bt, Chl, Ms, Qtz ± St.

[35] Thermobarometry was applied to sample UK06-62 (see Figure 7b for location), which shows a mineral assemblage the least retrogressed by D2 among all investigated amphibolite-grade samples. Major mineral phases and

Figure 9. Thin section and outcrop-scale observations from the Prosara inselberg. See Figure 6b for locations of the pictures. (a) Foliated granite showing solid-state deformation at low grade. Kf, alkali-feldspar; Qtz, quartz; sb, shear band; WM, white mica. Kf develops porphyroclasts with strong undulous extinction. The twinned Kf in the lower half of the picture shows quartz-filled fractures ("f"). Magmatic WM is only preserved in relics and has mostly recrystallized to fine-grained sericite along shear bands. Section is parallel to a weakly defined mineral aggregate lineation. Crossed nicols. (b and c) Mylonitic metasandstone parallel to an approximately N-S trending mineral aggregate lineation, indicating top-to-the-north directed transport. Quartz grains in the center of the picture show pronounced shape-preferred orientation and serrated grain boundaries indicative of bulging recrystallization. The fine-grained matrix consists of recrystallized quartz and white mica. Crossed nicols. Figure 9c shows detail of quartz aggregate from the mylonitic metasandstone in Figure 9b. The larger quartz grains show bulging recrystallization ("blg") and subgrains ("sg") and are surrounded by finer-grained recrystallized grains. Crossed nicols. (d) Asymmetrically sheared quartz aggregate deformed at semiductile conditions, indicating top-to-the-south directed transport. (e and f) Extensional shear bands developed at the brittle-ductile transition, indicating top-to-the-south directed transport. Bottom inset in Figure 9f shows stereographic representation of structural data. (g and h) Conjugate brittle faults crosscutting quartz rods and a metamorphic foliation. Bottom inset in Figure 9h shows stereographic representation of structural data. All plots are lower hemisphere, equal area projections.

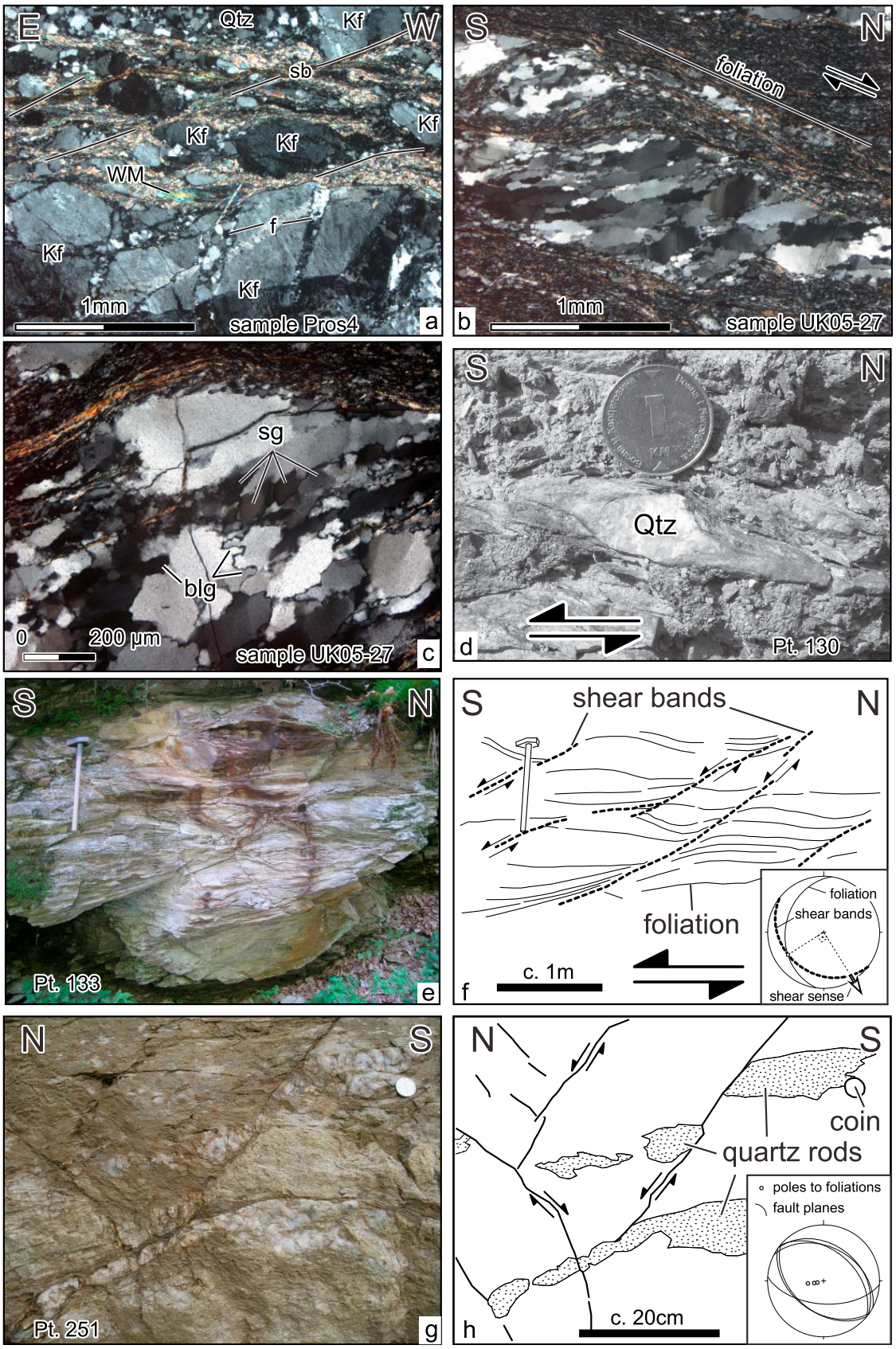
E
W
Qtz
Kf
sb
Kf
Kf
Kf
WM
f
Kf
Kf
1mm
sample Pros4
a
S
N
foliation
1mm
sample UK05-27
b
sg
blg
0
200 µm
sample UK05-27
c
S
N
Qtz
d
Pt. 130
S
N
Pt. 133
e
S
shear bands
N
foliation
c. 1m
f
foliation
shear bands
shear sense
N
S
Pt. 251
g
N
S
coin
quartz rods
poles to foliations
fault planes
c. 20cm
h

Figure 9

abundances in this sample are quartz, garnet (~1–2%), biotite (~10%), plagioclase (~10%), chlorite (~10%), white mica (~20%) and some staurolite (~1%). Ilmenite is the prevailing Ti phase. Garnet forms up to 1 mm large subhedral porphyroblasts with inclusions of quartz, biotite, muscovite, plagioclase and ilmenite (or possibly rutile). Representative chemical analyses of plagioclase, muscovite and biotite are given in Data Set S2. The microprobe traverses of garnet (Figures 12a and 12b) probably reveal a slight plateau in the garnet interior with a composition as follows: alm 76–79 mol %, spss 6–7 mo l%, py 7–8 mol %, grs 6–7 mol %. The compositional profile (Figure 12b) shows a rimward spss increase (20 mol %) and alm decrease (70 mol %). Pyrope and grossular abundances remain constant from core to rim. This zoning suggests retrogression ± garnet resorption probably during staurolite growth.

[36] An independent set of reactions obtained with the Thermocalc software 3.21 [*Holland and Powell*, 1998] (updated 2002) that uses measured mineral compositions as input (Data Set S2), yielded PT estimates of 630 ± 32°C and 6.8 ± 1.2 kbar. The GPMBQ-Fe-Mg geobarometer [*Hoisch*, 1990] gave 5.8–7.3 kbar at 600°C for the core. We are aware that these results should be treated with caution, since retrogression did probably also affect the garnet core composition. Hence, garnet growth was studied by means of pseudosection modeling carried out with the Theriak-Domino software [*de Capitani and Brown*, 1987] (also mainly the database of *Berman* [1988]) in the system Na_2O-K_2O-CaO-MgO-FeO-Fe_2O_3-MnO-Al_2O_3-SiO_2-TiO_2-H_2O-CO_2, using the bulk rock chemistry as input (Data Set S2). The P-T section (Figure 12c) predicts garnet growth at $p \geq 5$ kbar. The independently measured grs and alm isopleths of the garnet core (7 mol % grs, 76 mol % alm) intersect at ~600°C and 5–6 kbar. Also shown are the in isograds of staurolite, andalusite, sillimanite, as well as mineral assemblages of interest. Since monazite formation temperatures are ~550°C–600°C [*Krenn et al.*, 2008], the peak temperature and pressure conditions reached in the metapelites during D1 are estimated at 550°C to 630°C and 5 to 7 kbar. These results are widely consistent with pseudosection modeling obtained with the Perple_X thermodynamic software [*Connolly*, 2005] (version 07, using the internally consistent thermodynamic data set of *Holland and Powell* [1998], updated 2002; Figure S1).

4. Geochronology

4.1. U-Pb Dating

[37] Two igneous rock samples (see Figures 6a and 7d for sample locations) were analyzed by high-accuracy isotope dilution thermal ionization mass spectrometry (ID-TIMS) for dating zircon and monazite single crystals. Mineral separation and analytical techniques are given in section S1 of Text S1. The analytical results are presented in Figure S2 and Data Set S3.

[38] The sample from Prosara (UK04-02; Figure 9a; see Figure 6a for location) is a coarse-grained, leucocratic granite with a gneissic schistosity. It contained no monazite. The analyses of six zircons from this sample yielded a weighted mean $^{206}Pb/^{235}U$ age of 82.68 ± 0.13 Ma (Figure S2a).

[39] The sample from the Motajica intrusion (UK04-04; see Figure 7d for location) is a texturally isotropic granite. Analyses of seven zircons from this sample yielded a weighted mean $^{206}Pb/^{235}U$ age of 26.72 ± 0.10 Ma, while analyses of three monazites from the same sample gave a mean $^{207}Pb/^{235}U$ age of 26.64 ± 0.15 Ma (Figure S2b).

4.2. The $^{40}Ar/^{39}Ar$ Mineral Dating

[40] Amphibole and sericite concentrates, as well as illite-rich fine (2–6 and 6–12 μm) fractions were separated from samples taken from metamorphic units of Prosara and Motajica inselbergs. They were dated using the $^{40}Ar/^{39}Ar$ stepwise heating technique in order to constrain the cooling history of and/or the presence of synmetamorphic mineral growth in the studied units. Analytical procedures are given in section S1 of Text S1. The analytical results of all incremental heating experiments are presented in Figure 13 and Data Set S4.

[41] In Motajica inselberg we dated amphibole concentrates from two spatially separated occurrences of amphibolites and

Figure 10. Outcrop and thin section observations from the Motajica inselberg. See Figure 7 for locations. (a) Amphibolite facies mineral assemblages in metapelites. Plane polarized light. Bi, biotite; Qtz, quartz; St, staurolite; WM, white mica. Plane polarized light. (b) Garnet porphyroblast retrogressed at greenschist facies conditions. Plane polarized light. (c) Thin section micrograph of a granitoid foliated at solid state. The Kf porphyroclast in the center shows undulous extinction. Growth of epidote (Epi) is observed. Crossed nicols. (d) Growth of epidote at the expense of plagioclase indicating greenschist facies overprint of the granitoid. Plane polarized light. (e) Rotated garnet porphyroblast from an amphibolite-grade micaschist in a first metamorphic foliation s1, indicating top-to-the-SE directed sense of shear. Plane polarized light. (f) Mylonitic quartz layer associated with a first foliation s1. Pronounced shape-preferred orientation indicates top-to-the-SE directed sense of shear. Crossed nicols. (g and h) Transposition of s1 metamorphic foliation by a younger foliation s2 in metapelites. (i) Refolding of s1 foliation by s2 in amphibolite-grade metapelites. Here s1 is defined by a folded quartz layer and kinked white mica; s2 is subhorizontal. Newly formed biotite (Bi) along s2 suggests greenschist facies conditions during its formation. Plane polarized light. (j) Subhorizontal s2 crenulation cleavage in low-grade pelites. Plane polarized light. (k and l) White mica fish indicating top-to-the-west directed sense of shear in metapelites deformed under higher greenschist facies conditions. Crossed nicols. (m) Asymmetrically sheared quartz sigma clast in metapelites deformed at semiductile conditions, indicating top-to-the-west directed sense of shear. Coin for scale. (n) Extensional shear bands in metapelites, indicating top-to-the-east directed sense of shear. Coin for scale. (o) Stereographic representation of structural data collected at the site of Figures 10g and 10m. (p) Stereographic representation of structural data at the site of Figure 10n. All plots are lower hemisphere equal area projections.

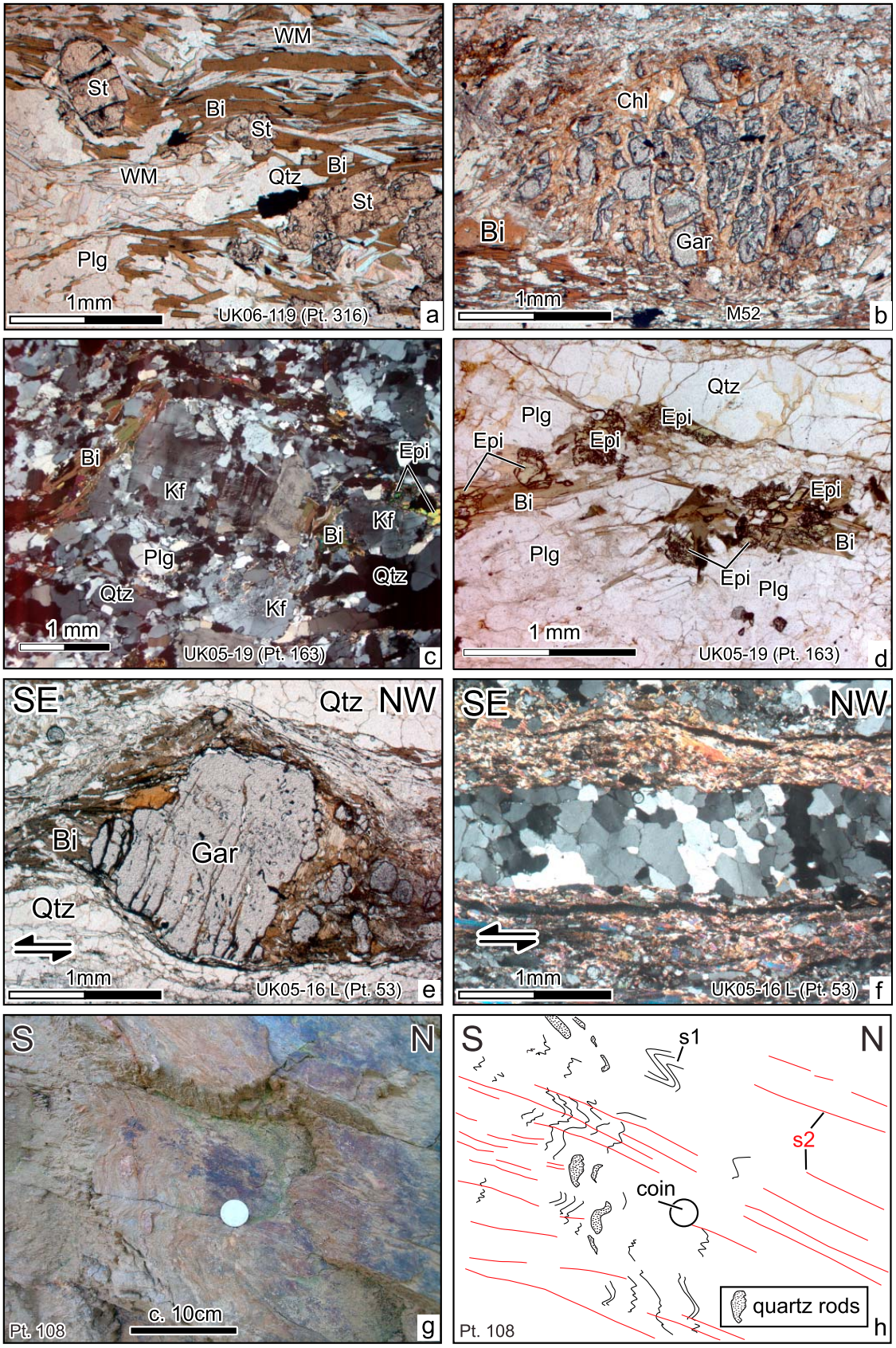
WM
St
Bi
St
WM
Qtz
Bi
St
Plg
1mm
UK06-119 (Pt. 316)
a
Chl
Bi
Gar
1mm
M52
b
Bi
Epi
Kf
Kf
Bi
Plg
Qtz
Qtz
Kf
1 mm
UK05-19 (Pt. 163)
c
Qtz
Plg
Epi
Epi
Epi
Epi
Bi
Bi
Plg
Epi
Plg
1 mm
UK05-19 (Pt. 163)
d
SE
Qtz
NW
Bi
Gar
Qtz
1mm
UK05-16 L (Pt. 53)
e
SE
NW
1mm
UK05-16 L (Pt. 53)
f
S
N
Pt. 108
c. 10cm
g
S
s1
N
s2
coin
quartz rods
Pt. 108
h

Figure 10

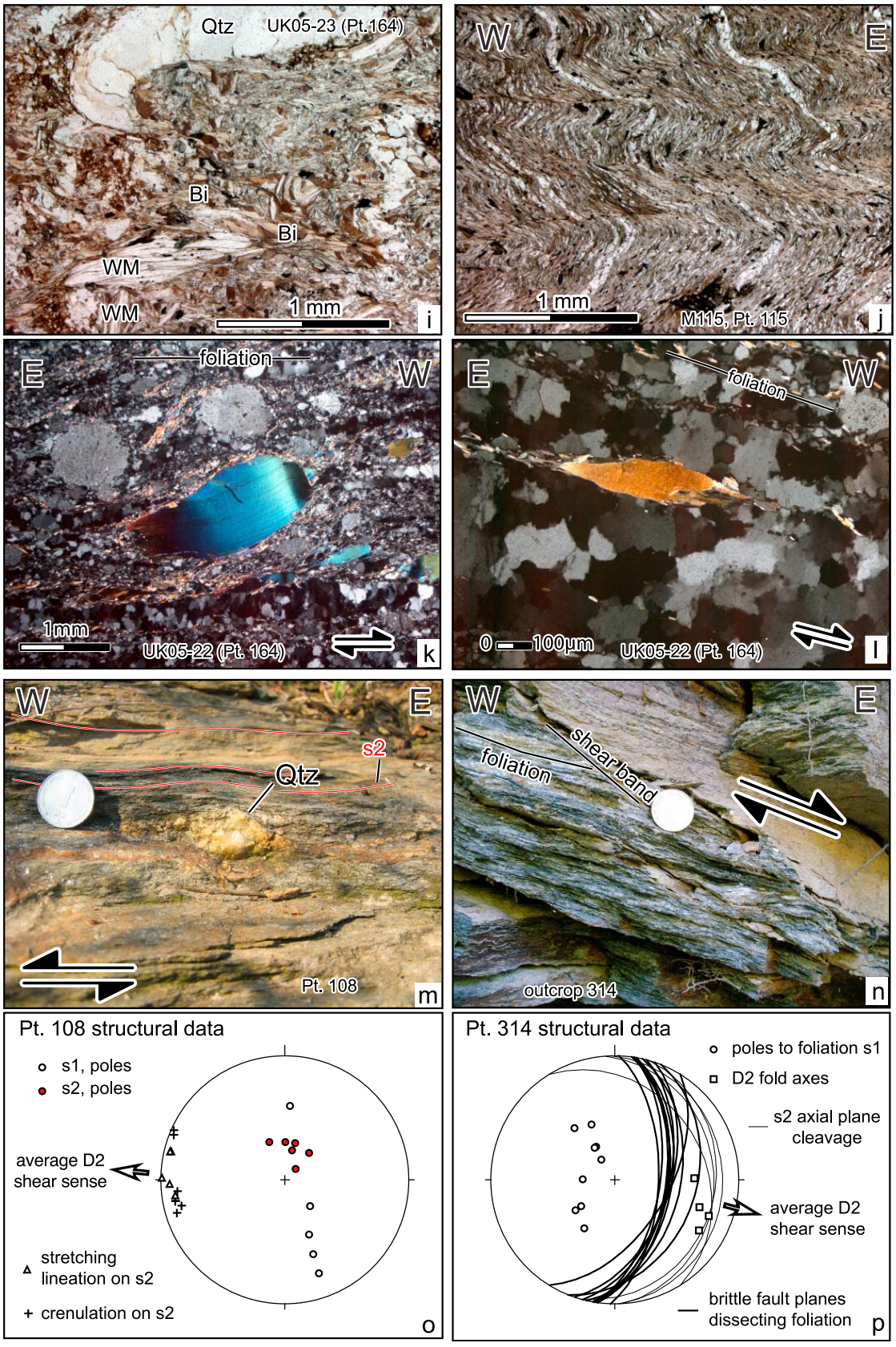

Figure 10. (continued)

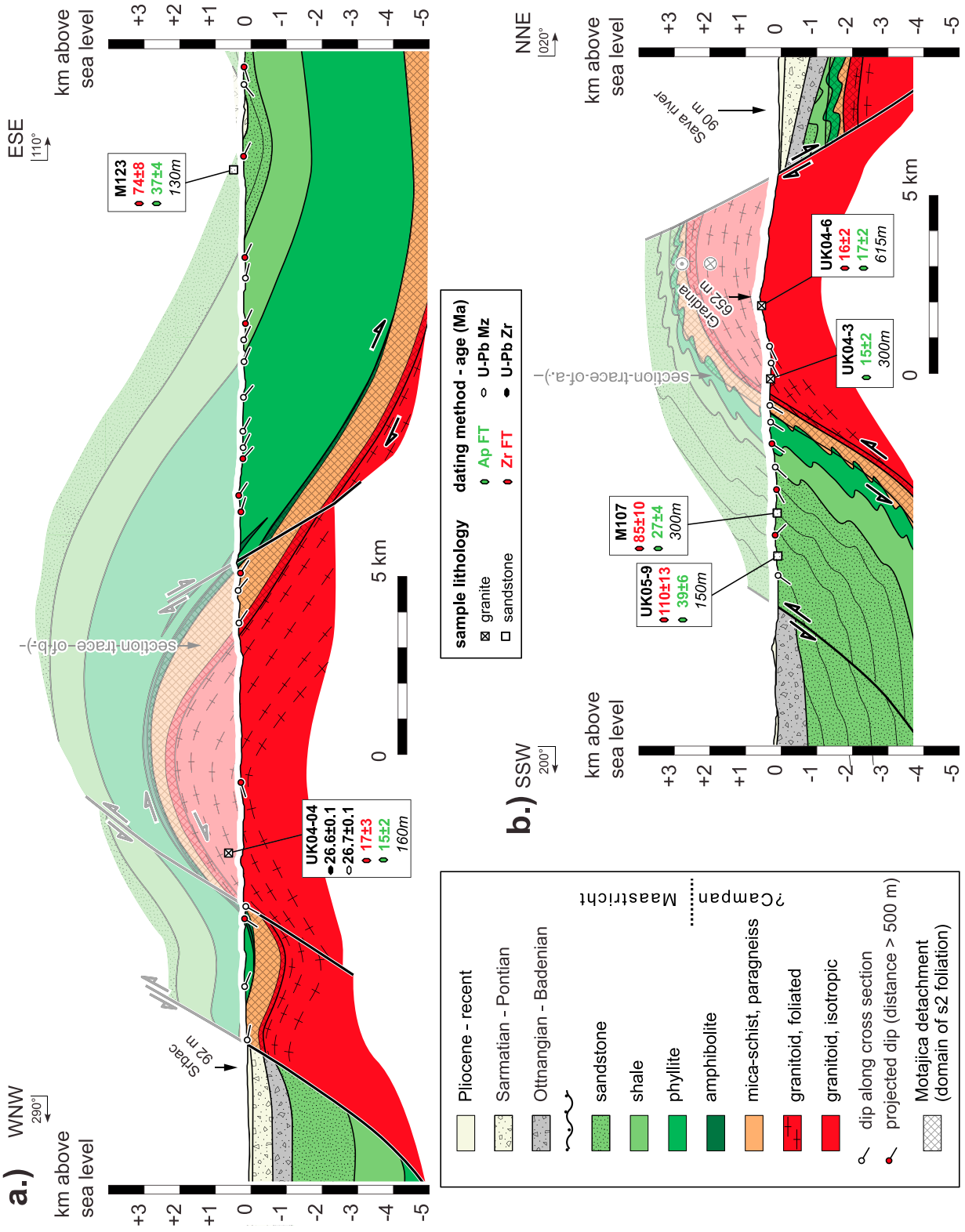

Figure 11. Interpretative geological (a) along-strike and (b) cross section through the Motajica inselberg. See Figure 7a for location of the sections.

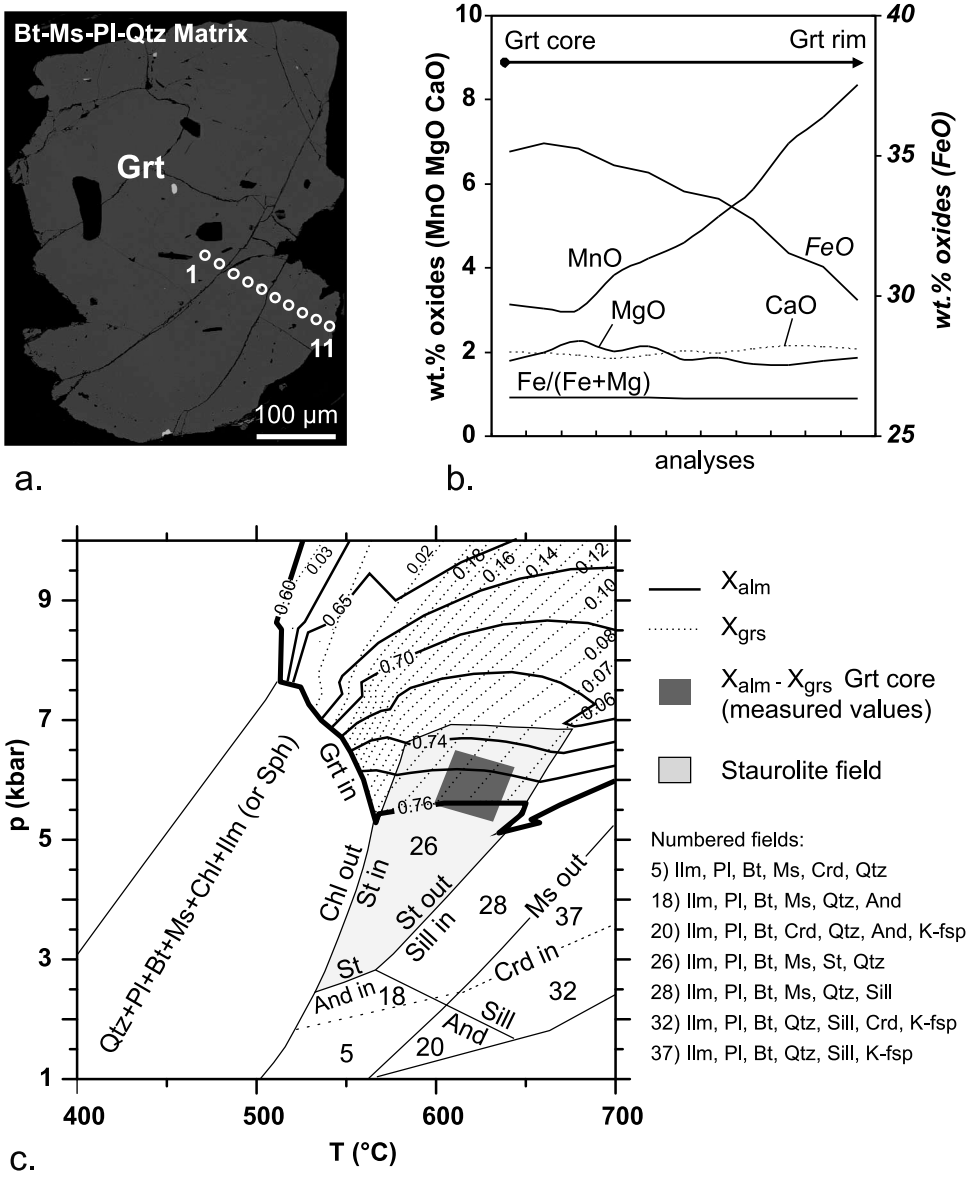

Figure 12. (a) Backscattered electron image and (b) chemical traverse of a garnet from sample UK06-62. (c) Staurolite and garnet stability field and garnet isopleths for the same sample according to the Theriak-Domino software [*de Capitani and Brown*, 1987]. The dark gray field corresponds to the intersection of measured garnet isopleths. See Figure 7b for sample location. Compare with Figure S1 for an independent but compatible P-T estimate.

epidote amphibolites (see Figure 7d for sample locations). The amphibole concentrates (samples M120a and M129) had K_2O contents between 0.1 and 0.4 wt % (see section S2 of Text S1, Figure S3 and Data Set S5 for further details on the mineral chemistry). Both samples M120a and M129 yielded nearly identical ages for about 80–90% of the total ^{39}Ar released. This resulted in plateau ages of 58 ± 6 Ma and 53 ± 5 Ma, respectively (Figures 13a and 13b). The total gas ages for the same two samples were ~63 ± 7 Ma and 52 ± 5 Ma, respectively.

[42] In Prosara inselberg, we dated a handpicked sericite aggregate and a sericite fine fraction from a foliated calcite marble (sample UK06-58; see Figure 6a for location), regarded as representing a newly grown mineral phase. The sericite aggregates were taken from millimeters thin sericite layers embedded in the marble that grew in s1 and which later became crenulated; they consist of intergrown muscovite and chlorite with an average grain size between ~20 and 100 μm (see section S2 of Text S1 and Figure S4 for further details). The fine fraction mostly consisted of muscovite and clinochlore according to XRD analysis; no other low-K clay minerals (e.g., kaolinite or smectite) were identified. The handpicked sericite aggregate gave a plateau age of ~25 ± 1.5 Ma corresponding to 32% of the total ^{39}Ar released and a total gas age of 26 ± 1 Ma (Figure 13c). The

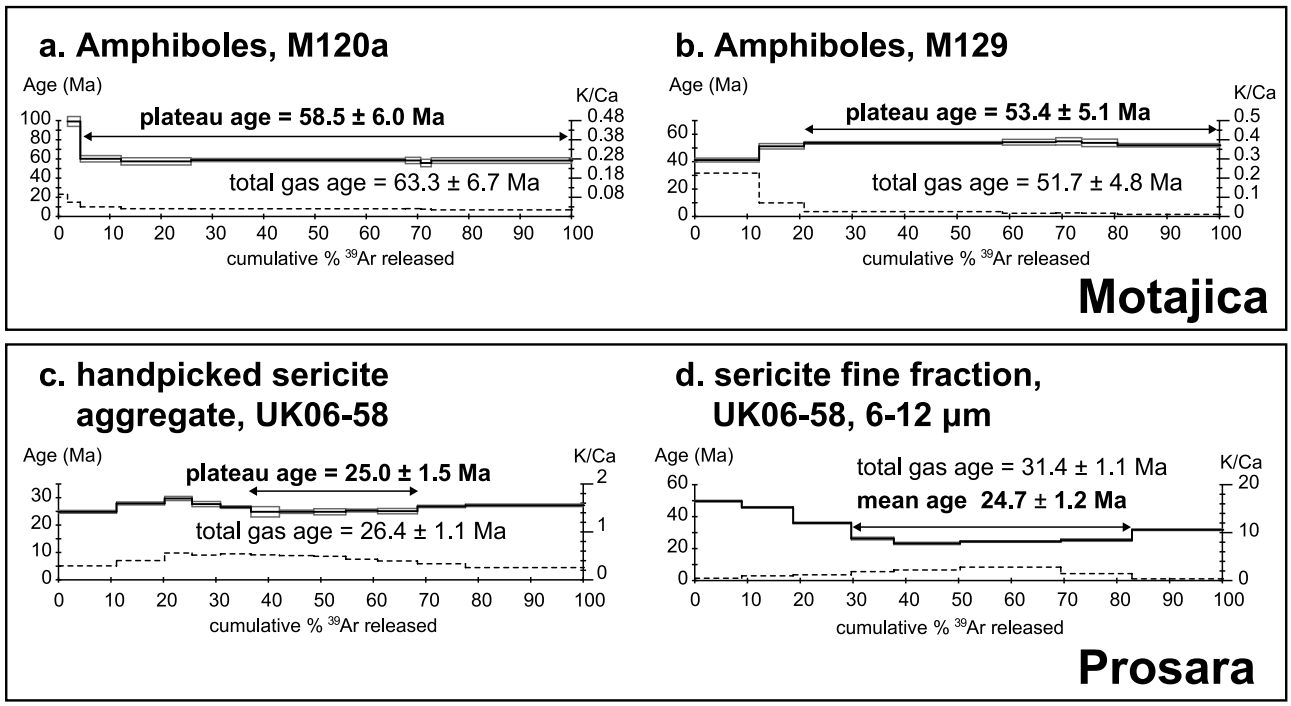

Figure 13. (a–d) Shown are $^{40}Ar/^{39}Ar$ incremental release spectra of mineral concentrates and sericite fine fractions from the Motajica and Prosara inselbergs. Experimental temperatures increase from left to right. Analytical uncertainties are shown by the vertical width of the horizontal bars. Dashed line represents the K/Ca ratio. See Figures 6 and 7 for sample locations.

6–12 μm size fraction (Figure 13d) showed decreasing age steps up to 30% of the total ^{39}Ar released, followed by four stages with fairly constant ages between 23 and 26 Ma; a final heating increment yielded an age of 32 Ma. Those fairly constant stages define a mean age of ~24.7 ± 1 Ma, corresponding to 53% of the total ^{39}Ar released. The total gas age of this sample is 31 ± 1 Ma.

4.3. Zircon and Apatite Fission Track Analysis

[43] Zircon and apatite fission track (FT) analyses were performed on a range of samples from inselbergs in Bosnia and Hercegovina (Kozara, Prosara and Motajica), Croatia (Papuk-Psunj) and western Serbia (Cer). The geographic locations of the samples and analytical results are shown in Figures 3, 5, 6a, 7d and 8. Detailed analytical results are presented in Table 1. Analytical procedures are described in section S1 of Text S1. Apatite fission track modeling was performed on selected samples (Figure 14) (see section S3 of Text S1 for a description of the technique).

4.3.1. Prosara Inselberg

[44] The granitic gneiss sample that gave a Campanian crystallization age (UK04-02; Figure 6a and Figure S2a, see section 4.1), yielded zircon and apatite FT ages of 21 ± 2 Ma and 17 ± 2 Ma, respectively. Only two horizontal confined tracks could be observed in this sample (Table 1).

4.3.2. Motajica Inselberg

[45] We analyzed three samples from the Motajica pluton and three samples from the nonmetamorphic Maastrichtian sandstones (Figure 7d and Table 1). The granite samples yielded zircon FT ages of 17 ± 2 Ma (UK04-04) and 16 ± 2 Ma (UK04-06), respectively. The apatite FT ages range between 17 ± 2 Ma and 15 ± 2 Ma (UK04-06, UK04-04, and UK04-03). Only 20 confined track lengths were measured in all three samples, which did not allow meaningful modeling of the data; the mean track length is 14.35 ± 0.2 μm with a standard deviation of 0.69 μm. The three Maastrichtian sandstone samples (UK05-09, M107, and M123) yielded zircon FT ages between 110 ± 13 Ma and 74 ± 8 Ma. The apatite FT ages range between 39 ± 6 Ma and 27 ± 4 Ma with mean track lengths between 14.53 and 14.14 μm and standard deviations between 1.37 and 1.04 μm.

4.3.3. Cer Inselberg

[46] A sample taken from a two-mica granite (UK04-08; Figure 8) yielded an apatite FT age of 14 ± 1 Ma. Nineteen confined tracks could be measured with mean track lengths of 14.77 ± 0.1 μm and a standard deviation of 0.56 μm (Table 1).

4.3.4. Papuk Inselberg

[47] A granite sample from the Paleozoic basement (UK06-28; Figure 3) yielded a zircon FT age of 135 ± 8 Ma. The apatite FT age was 43 ± 6 Ma. 102 confined tracks measured gave a mean track length of 14.21 ± 0.1 μm and a standard deviation of 1.42 μm (Table 1).

4.3.5. Kozara Inselberg

[48] Five zircon and two apatite samples were dated from ophiolites and their Maastrichtian to Mid-Eocene sedimentary cover (Figures 3 and 5 and Table 1). One dolerite

Table 1. Zircon and Apatite Fission Track Dating Results of Samples From Different Inselbergs in the Sava Zone[a]

	Grid References[b]	Alt. (m)	Lithology	Strat. Division	Number of Grains	ρd (Nd) ($\times10^6$ cm^{-2})	ρs (Ns) ($\times10^6$ cm^{-2})	ρi (Ni) ($\times10^6$ cm^{-2})	P (χ2) (%)	U. conc. (ppm)	Central Age (±2σ) Ma	MTL (±1σ) (μm)	SD (N) (μm)	Dpar[c] (μm)
						Motajica								
Sample UK04-04														
Apatite	*6470599/4994337*	*160*	*granite*	*Motajica granite*	*24*	*0.964 (5,746)*	*0.129 (258)*	*1.390 (2,774)*	*95*	*17*	*15.2 ± 2.2*	*14.83 ± 0.35*	*0.31 (3)*	*1.57*
Zircon	*6470599/4994337*	*160*	*granite*	*Motajica granite*	*6*	*0.378 (2,887)*	*12.329 (361)*	*16.974 (497)*	*78*	*1512*	*16.7 ± 2.4*	*14.83 ± 0.35*	*0.31 (3)*	*1.57*
Sample UK04-06														
Apatite	*6473918/4994260*	*615*	*granite*	*Motajica granite*	*22*	*0.880 (5,746)*	*0.218 (254)*	*1.978 (2,302)*	*92*	*28*	*16.5 ± 2.4*	*14.25 ± 0.19*	*0.69 (13)*	*1.48*
Zircon	*6473918/4994260*	*615*	*granite*	*Motajica granite*	*9*	*0.445 (2,887)*	*5.098 (311)*	*8.459 (516)*	*100*	*613*	*16.3 ± 2.2*	*14.25 ± 0.19*	*0.69 (13)*	*1.48*
Sample UK04-03														
Apatite	*6473013/4992348*	*300*	*granite*	*Motajica granite*	*20*	*0.981 (5,746)*	*0.271 (432)*	*3.006 (4,785)*	*54*	*38*	*14.7 ± 1.6*	*14.32 ± 0.33*	*0.66 (4)*	*1.56*
Sample UK05-09														
Apatite	6470132/4989036	150	arkose	Maastrichtian	20	1.239 (8,099)	0.833 (279)	4.469 (1,497)	22	74	38.6 ± 6.4	14.53 ± 0.23	1.05 (21)	1.61
Zircon	6470132/4989036	150	arkose	Maastrichtian	27	0.414 (2,887)	15.759 (1,788)	3.578 (406)	100	286	110.0 ± 13.4	14.53 ± 0.23	1.05 (21)	1.61
Sample M107														
Apatite	6478532/4985905	300	arkose	Maastrichtian	22	0.971 (7,207)	0.447 (207)	2.657 (1,230)	96	33	27.1 ± 4.2	14.14 ± 0.14	1.37 (101)	2.1
Zircon	6478532/4985905	300	arkose	Maastrichtian	24	0.433 (2,887)	6.775 (1,678)	2.100 (520)	100	156	84.5 ± 9.6	14.14 ± 0.14	1.37 (101)	2.1
Sample M123														
Apatite	6486754/4984297	130	arkose	Maastrichtian	19	0.955 (7,207)	0.715 (481)	3.036 (2,043)	97	40	37.3 ± 4.2	14.40 ± 0.12	1.04 (76)	2.1
Zircon	6486754/4984297	130	arkose	Maastrichtian	21	0.417 (2,887)	11.573 (2,026)	3.941 (690)	97	348	74.1 ± 7.6	14.40 ± 0.12	1.04 (76)	2.1
						Prosara								
Sample UK04-02														
Apatite	*6427995/5004697*	*100*	*granite gneiss*	*late Cretaceous granite*	*22*	*1.015 (5,746)*	*0.3258 (274)*	*3.335 (2,811)*	*58*	*39*	*16.8 ± 2.4*	*14.64 ± 0.04*	*0.06 (2)*	*1.8*
Zircon	*6427995/5004697*	*100*	*granite gneiss*	*late Cretaceous granite*	*18*	*0.391 (2,887)*	*9.122 (1,083)*	*10.186 (1,224)*	*93*	*831*	*21.0 ± 2.0*	*14.64 ± 0.04*	*0.06 (2)*	*1.8*
						Kozara North								
Sample K149zr														
Zircon	6413654/4993906	175	dolerite	N. Kozara ophiolites	10	0.428 (2,887)	16.541 (1,120)	7.606 (515)	98	598	56.4 ± 6.8			
Sample K150zr														
Zircon	6419208/4992483	260	gabbro	N. Kozara ophiolites	12	0.427 (2,887)	10.312 (1,170)	4.354 (494)	99	355	61.2 ± 7.4			
Sample K146zr														
Zircon	6410911/4992754	300	granite clast	Maastrichtian–Lower Paleocene	20	0.425 (2,887)	22.011 (2,108)	9.899 (948)	96	741	57.3 ± 5.4			
Sample UK06-02														
Apatite	6424458/4988255	250	sandstone	Upper Paleocene–Eocene	21	1.364 (11,383)	0.220 (113)	1.747 (898)	100	17	28.5 ± 5.8	14.81 ± 0.22	0.44 (4)	2.35
Zircon	6424458/4988255	250	sandstone	Upper Paleocene–Eocene	32	0.433 (2,471)	10.144 (2,636)	3.437 (893)	76	265	77.3 ± 3.7	14.81 ± 0.22	0.44 (4)	2.35
Sample UK06-09														
Apatite	6415260/4989980	550	sandstone	Maastrichtian–Lower Paleocene	23	1.318 (11,383)	0.073 (73)	0.381 (384)	100	4	41.5 ± 10.8			2.59
						Kozara South								
Sample K135zr														
Zircon	6411224/4983890	315	dolerite	S. Kozara ophiolites	7	0.401 (2,887)	8.156 (398)	2.049 (100)	97	175	96.4 ± 22.2			
						Papuk								
Sample UK06-28														
Apatite	6450760/5045230	275	granite	Paleozoic granite	20	1.147 (11,383)	0.513 (298)	2.286 (1,328)	96	23	42.6 ± 5.8	14.21 ± 0.14	1.42 (102)	2.08
Zircon	6450760/5045230	275	granite	Paleozoic granite	19	0.438 (2,471)	12.17 (2,287)	2.385 (448)	98	187	134.7 ± 7.9	14.21 ± 0.14	1.42 (102)	2.08
						Cer								
Sample UK04-08														
Apatite	*6613033/4944171*	*250*	*granite*	*Cer granite*	*23*	*0.813 (5,746)*	*0.438 (699)*	*4.413 (7,043)*	*97*	*66*	*13.7 ± 1.4*	*14.77 ± 0.13*	*0.56 (19)*	*1.44*

[a]Samples from the footwall of Neogene detachments are shown in italics. Analyst is A. Kounov.
[b]Grid references are MGI Balkan 6 coordinates.
[c]Between 5 and 10 etch pits were measured per dated grain, depending on the quality and the density of the track pits on the grain surface.

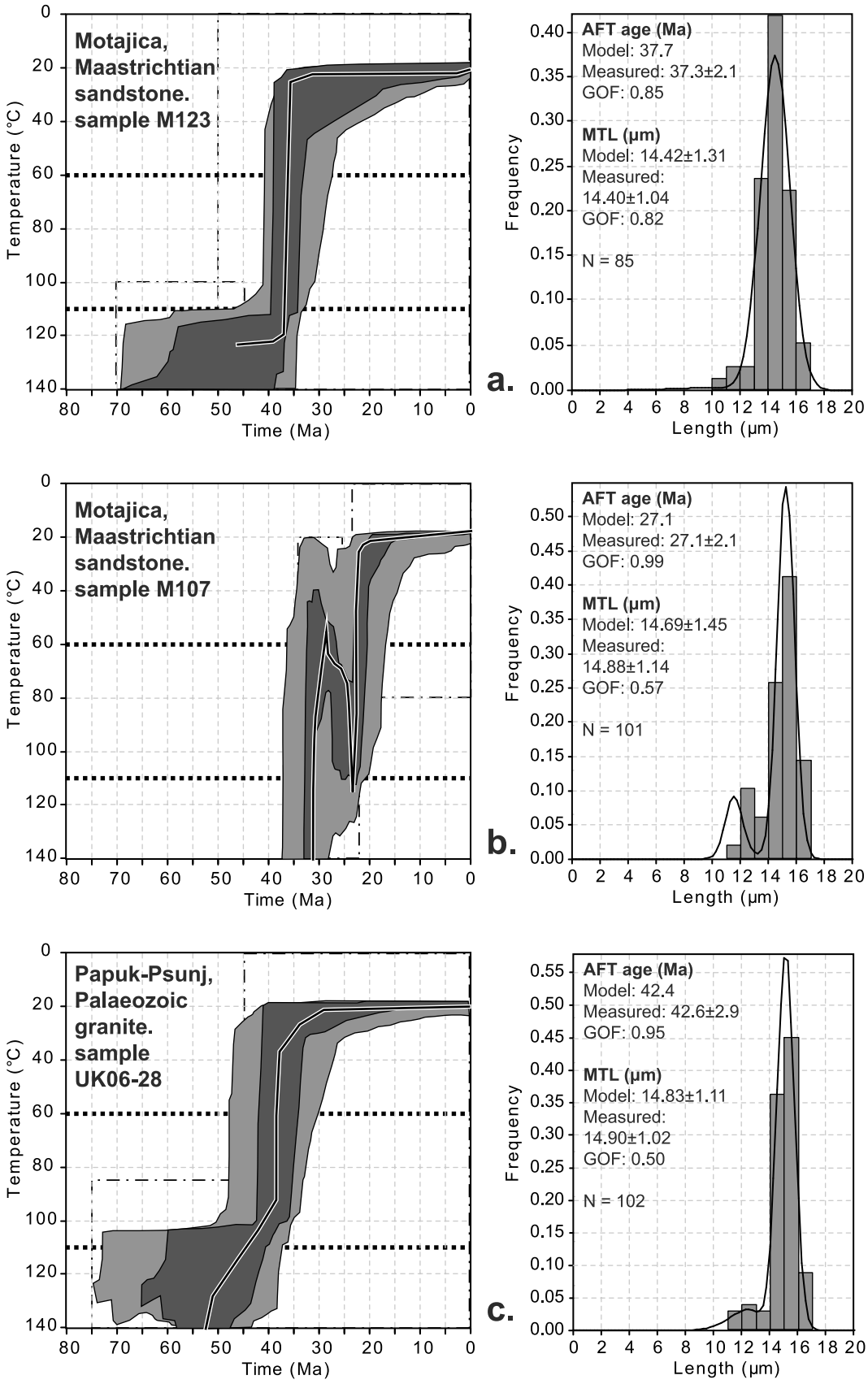
Motajica,
Maastrichtian
sandstone.
sample M123
Temperature (°C)
Time (Ma)
AFT age (Ma)
Model: 37.7
Measured: 37.3±2.1
GOF: 0.85
MTL (µm)
Model: 14.42±1.31
Measured:
14.40±1.04
GOF: 0.82
N = 85
Frequency
Length (µm)
a.
Motajica,
Maastrichtian
sandstone.
sample M107
AFT age (Ma)
Model: 27.1
Measured: 27.1±2.1
GOF: 0.99
MTL (µm)
Model: 14.69±1.45
Measured:
14.88±1.14
GOF: 0.57
N = 101
b.
Papuk-Psunj,
Palaeozoic
granite.
sample
UK06-28
AFT age (Ma)
Model: 42.4
Measured: 42.6±2.9
GOF: 0.95
MTL (µm)
Model: 14.83±1.11
Measured:
14.90±1.02
GOF: 0.50
N = 102
c.

Figure 14

(K149) and one gabbro sample (K150) from the northern Campanian-age ophiolitic complex yielded zircon FT ages of 56 ± 7 Ma and 61 ± 7 Ma, respectively. A granite boulder taken from Maastrichtian conglomerates that overlie this Campanian magmatic succession (K146) yielded a zircon FT age of 57 ± 5 Ma. Sample UK06-09 from another Maastrichtian sandstone yielded an apatite FT age of 42 ± 11 Ma (Figure 5). No horizontal confined tracks could be measured for this sample. Dolerite sample K135 from the southern (Jurassic) ophiolite complex yielded a zircon FT age of 96 ± 22 Ma (Figure 5). The intrusion age of this dolerite is unknown, but very likely Late Jurassic, as inferred from spatially adjacent gabbros dated at 158 ± 8 Ma [*Ustaszewski et al.*, 2009]. Sample UK06-02 from the Eocene turbiditic sandstones yielded a zircon FT age of 77 ± 7 Ma and an apatite FT age of 29 ± 6 Ma (Table 1).

5. Interpretation of Geochronological and Structural Data

5.1. Interpretation of U-Pb Ages From Magmatic Rocks

[49] The Campanian zircon dates (82.68 ± 0.13 Ma; Figure S2a) are interpreted to constrain the crystallization age of the Prosara granite, which is in good agreement with the reported age of other felsic magmatics from Moslavačka Gora [*Balen et al.*, 2001; *Starijaš et al.*, 2004, 2006, 2010] and Požeška Gora [*Pamić et al.*, 1988]. Crystallization of the Prosara granite is also coeval with Campanian-age bimodal magmatics in the ophiolitic complex of North Kozara [*Ustaszewski et al.*, 2009]. Since our observations show that the dated Prosara granite is overprinted by a solid state foliation that is concordant with the foliation within the surrounding phyllites, this crystallization date also provides an upper time bracket for regional deformation and metamorphism in the Prosara area.

[50] The new U-Pb zircon and monazite ages of around 26.7 Ma obtained for the Motajica granite (Figure S2b) are in disagreement with a previously reported Rb-Sr whole rock isochron age of around 48 Ma for this granite [*Lanphere and Pamić*, 1992]. For methodological reasons we regard our new data as more reliable for dating the intrusion; also the age reported by our study is in better agreement with all the other geochronological data available from Motajica inselberg further discussed below. Possibly, the 48 Ma Rb-Sr age reflects mixing of Late Oligocene anatectic granitic melts with older crustal components.

5.2. Interpretation of $^{40}Ar/^{39}Ar$ Mineral Ages From Metamorphic Rocks

[51] Plateau ages (58 ± 6 Ma and 53 ± 5 Ma) and total gas ages (63 ± 7 Ma and 52 ± 5 Ma) obtained from amphibole concentrates from Motajica (M120a and M129; Figure 13a and 13b) coincide within analytical uncertainties, which indicates that the plateau ages are statistically viable. In the case of sample M120a the constant K/Ca ratios throughout all heating steps suggest degassing of a compositionally homogeneous mineral phase. In sample M129, the K/Ca ratio continuously decreased with progressive heating, indicating compositional zoning of the amphiboles. This is in agreement with evidence from the chemical analyses of the amphiboles (section S2 of Text S1). Since D1 peak metamorphic conditions in the spatially closely associated amphibolite facies metapelites reached temperatures between 550°C and 630°C according to our petrological data, and by assuming the commonly accepted range of closure temperatures for amphiboles in the $^{40}Ar/^{39}Ar$ system somewhere between 480°C and 530°C [e.g., *Harrison and McDougall*, 1980; *Berger and York*, 1981], the obtained plateau ages can be regarded as dating early cooling below about 500°C some 55 Ma ago. This is in agreement with the less accurate chemical Th-U-Pb monazite ages of 63 ± 9 Ma obtained from amphibolite-grade metapelites in the same area [*Krenn et al.*, 2008] (Figure 7d). The latter are interpreted to date D1 peak temperature conditions, since the metamorphic peak temperatures were lower than the closure temperature for monazite in the U-Pb system (>700°C [e.g., *Mezger*, 1990]). The new amphibole $^{40}Ar/^{39}Ar$ cooling ages reported here, in combination with the Maastrichtian stratigraphic age of the protolith (between 70.6 and 65.5 Ma [*Gradstein et al.*, 2004]) indicate that D1 peak metamorphic conditions were reached after 70.6 and before 55 Ma ago, i.e., at around the Cretaceous-Cenozoic boundary.

[52] The handpicked sericite aggregate from the greenschist facies calcite marble from Prosara (sample UK06-58) yielded a plateau age of 25 ± 1.5 Ma (Figure 13c). The sericite fine fraction of the same sample (Figure 13d) shows decreasing age steps up to ~30% ^{39}Ar released, indicating either degassing of different mineral reservoirs, possible excess ^{40}Ar or recoil of ^{39}Ar at grain rims. All subsequent heating steps gave a mean age of 24.7 ± 1 Ma, which summed up to 53% of ^{39}Ar released. A continuously decreasing staircase pattern throughout all heating steps, suggesting rims being older than cores, was not observed. We hence presume that ^{39}Ar recoil did not dominate the entire release spectrum. Both in the case of the handpicked

Figure 14. Results of apatite fission track modeling of samples (a) M123 and (b) M107 in the hanging wall of the Motajica detachment and (c) sample UK06-28 from the Paleozoic basement of the Tisza-Dacia Mega-unit. See Figures 3 and 7 for sample locations. The thin dash-dotted lines limit the user-defined time (t)-temperature (T) boxes. Thick horizontal dashed lines within individual models at 60°C–110°C bracket the partial annealing zone (PAZ) for apatite within the temperature limits assigned by *Laslett et al.* [1987]. The thick solid black lines represent the best fit paths. The light gray shading highlights the area defined by the "acceptable" thermal history paths corresponding to the goodness of fit value (GOF) > 0.05. The dark gray shading highlights the area defined by the "good" thermal history paths corresponding to the goodness of fit value > 0.5 (for details see section S3 of Text S1). MTL, mean track length; N, number of horizontal confined tracks measured.

sericite aggregate and the fine fraction, relatively constant K/Ca ratios throughout all heating steps defining the plateau and mean age suggest degassing of compositionally homogeneous mineral phases. All this evidence shows that the isotopic system did not close before some 25 Ma. Mineral assemblages (Figure 6a) suggest that middle to upper greenschist facies were reached within the Prosara metamorphic unit. Quartz microstructures related to D2 indicate temperatures in the range of 350°C to 450°C (Figure 9). This is within the range of the $^{40}Ar/^{39}Ar$ white mica closure temperature between ~380°C and 400°C for cooling rates between 1°C and 10°C/Ma and a grain size of 100 μm [*Harrison et al.*, 2009]. We hence interpret the $^{40}Ar/^{39}Ar$ white mica ages around 25 Ma as dating the cooling of the metamorphics related to extensional unroofing during D2.

5.3. Interpretation of Fission Track Ages

[53] Structural and fission track data from the Motajica inselberg document the existence of two structural domains with contrasting thermal histories during a Late Oligocene to Miocene extension event. These two domains are separated by what we interpret as an extensional low-angle detachment, termed Motajica detachment (Figures 7c and 7d). The ~27 Ma old Motajica granite and its greenschist- to amphibolite-grade metamorphic frame were exhumed from below this detachment. Our fission track ages constrain the onset of extension between the time of granite emplacement (27 Ma) and deposition of the earliest Neogene synrift sediments in the Sava depression (Ottnangian, ~18.3 Ma [*Pavelić*, 2001; *Saftić et al.*, 2003]). All fission track ages obtained from the hanging wall of this detachment predate granite intrusion (Figure 7d). In the following discussion we hence separated our fission track data set into two subsets obtained from below and above the Motajica detachment, respectively. Based on already presented structural and geochronological data we further assume that the Motajica detachment exposed in the Motajica inselberg must be part of a much larger low-angle detachment or detachment system, which originally extended across several inselbergs and that is now disrupted by younger high-angle normal (possibly transtensional) faults and/or covered by Neogene strata. Following this logic we also separated fission track data obtained in adjacent inselbergs into footwall and hanging wall of a larger Motajica detachment.

5.3.1. Fission Track Data From the Footwall of the Detachment

[54] The zircon and apatite FT ages in the footwall of the Motajica detachment are very close to each other, especially when considering their relative errors (Figure 7d). Hence, a very fast cooling through the zircon and apatite FT closure temperatures (300°C–60°C) is suggested for the 17 to 15 Ma time interval. The rather long mean track length of 14.35 ± 0.2 μm (Figure 7d, bottom inset) measured for all three Motajica granite samples (only 20 confined tracks measured for all three), also suggests relatively fast cooling through the apatite partial annealing zone (110°C–60°C).

[55] The greenschist facies Prosara metamorphics yielded a zircon FT age of 21 ± 1 Ma (Figure 6a). Together with the structural data and the $^{40}Ar/^{39}Ar$ cooling ages of ~25 Ma, this indicates that the Prosara metamorphics were also located in the footwall of the larger Motajica detachment. Hence extension-related cooling also affected the Prosara inselberg and probably commenced between 25 and 21 Ma.

[56] The Cer inselberg (Figure 8) reflects a cooling and exhumation history that is expected for the footwall rocks of the larger Motajica detachment when combining the apatite FT age of ~14 ± 1 Ma, obtained from an S-type two-mica granite, with the K-Ar ages of K-spar (16.48 ± 0.62 Ma), biotite (17.22 ± 0.66 Ma) and amphibole (21.11 ± 1.66 Ma) reported from a quartz monzonite nearby [*Knežević et al.*, 1994a]. Thus we propose that following crystallization of the quartz monzonite, the Cer two-mica granite intruded between 19 and 16 Ma ago [*Koroneos et al.*, 2010] into the footwall of the larger Motajica detachment and rapidly cooled through the apatite partial annealing zone ~14 Ma ago. Furthermore the coeval rapid cooling in the Prosara and Motajica areas together with the structural data indicate that fast cooling was extension related and affected an area of at least 150 km (distance between Motajica and Cer) along the southern rift margin of the Pannonian basin, leading to Ottnangian to Badenian rift-related subsidence (~18.3 to 13 Ma [*Pavelić*, 2001; *Saftić et al.*, 2003]).

5.3.2. Fission Track Data From the Hanging Wall of the Detachment

[57] Modeling of apatite FT data from the Maastrichtian sediments in the hanging wall of the Motajica detachment shows a totally different thermal history compared to the samples from the footwall (Figure 14). These rocks show an earlier phase of fast cooling between 40 and 35 Ma (samples M123 and M107; Figures 14a and 14b). Owing to the lack of evidence for any extensional structures other and older than the Motajica detachment, this cooling could be due to accelerated hanging wall erosion during southwestward thrusting of this unit onto more external units after ~40 Ma. Such thrusts are directly evidenced in Kozara Mountain (Figure 5). The short-lived heating event between 28 and 23 Ma, modeled in sample M107, can best be related to the emplacement of the 27 Ma old Motajica granite (Figure 14b).

[58] Zircon FT central ages from the Maastrichtian sandstones from Motajica inselberg (samples UK05-09, M107 and M123, 110 to 74 Ma) are slightly older than, or statistically overlap with the sedimentation age, suggesting that they represent detrital ages. The analyzed samples passed the $P\chi^2$ test. Based on statistical arguments these central ages therefore present single populations. However, single grain ages are equal to or older than the Maastrichtian depositional age with a relatively large spread (Figure S5). This led us to consider the central ages as possibly presenting a mixture of different detrital populations with similar ages. The zircon grains within the analyzed samples are exclusively euhedral and yielded FT ages that coincide with Late Cretaceous volcanism reported from Kozara [*Ustaszewski et al.*, 2009] and Papuk-Psunj [e.g., *Pamić*, 1993b; *Pamić et al.*, 2000]. Such euhedral zircons must have experienced only short transport and mechanical abrasion and could therefore represent detrital minerals derived directly from volcanic islands of the Sava Zone and/or from Andean-type volcanoes in the Tisza-Dacia Mega-

unit. A relatively older population within the same set of three samples (UK05-09, M107 and M123) yielded single grain ages between 150 and 110 Ma (Figure S5). This is close to the zircon FT central age of 135 ± 16 Ma obtained on the Paleozoic granite from Papuk Mountain (sample UK06-28; Figure 3) and indicates possible direct sourcing from the basement of the Tisza-Dacia Mega-unit. The maximum temperatures of the Maastrichtian sediments, estimated from illite and chlorite crystallinity, is 200°C–300°C (section 3.2), corresponding to the zircon FT closure temperature. Considering the statistical fit of the single grain ages with possible source ages (Figure S5 and above), full resetting or even considerable reduction of the zircon FT ages in these samples is excluded.

[59] Zircon and apatite FT data obtained from North Kozara (Figure 5) show that this area also is part of the hanging wall above the larger Motajica detachment. Zircon FT central ages from the Campanian North Kozara ophiolite (samples K149 and K150) and its Maastrichtian cover sediments (sample K146) range between 61 and 56 Ma (Figure 5). The sampled Campanian magmatics are shallow subvolcanics that must have been close to the surface at the time of crystallization; they are reworked in the Maastrichtian cover [*Ustaszewski et al.*, 2009]. This suggests that this succession had an either tectonic or sedimentary overburden high enough for fully resetting the zircon FT system (~250°C). Sedimentary overburden is unlikely, because the southerly adjacent Late Paleocene to Mid-Eocene sediments were deposited between about 59 and 40 Ma (Thanetian to Lutetian; Figure 4), i.e., later than the suggested heating event. Hence, tectonic overburden provided by the Tisza-Dacia Mega-unit, more likely explains the reset zircon FT ages. Heating must have occurred probably before ~61 Ma and was followed by cooling and closure of the zircon FT system between 61 and 56 Ma. These ages are similar to the amphibole $^{40}Ar/^{39}Ar$ data obtained from the structurally deeper footwall of the Motajica detachment in Motajica inselberg that indicate cooling from peak metamorphism to below ~500°C around 55 Ma.

[60] The apatite FT central age of 42 ± 11 Ma obtained on the Maastrichtian sandstone from North Kozara (sample UK06-09; Figure 5) is similar to the reset apatite FT central ages obtained from the Maastrichtian sandstones in the hanging wall of the Motajica detachment (samples UK05-09, M107 and M123; Figure 7d). Cooling of the North Kozara unit (i.e., Campanian ophiolite and Maastrichtian cover) to temperatures below the apatite FT closure temperature (110°C ± 10°C) is interpreted, in analogy to Motajica, as related to thrusting onto the more external Paleogene sediments (outcropping between North and South Kozara; Figure 5) and concomitant hanging wall erosion. The apatite FT central age of 29 ± 6 Ma obtained on a sandstone from this succession (sample UK06-02; Figure 5) is younger than the depositional minimum age (Lutetian, ~40 Ma) and hence reset. This demonstrates that this succession was also buried to temperatures high enough for resetting the apatite FT system, likely due to underthrusting below the northerly adjacent units. Cooling of this succession below the apatite closure temperature took place after 29 ± 6 Ma, i.e., later than the tectonically higher units farther north in Motajica inselberg. The same sample UK06-02 yielded a zircon FT central age of 77 ± 7 Ma with a wide range of single grain ages between 120 and 55 Ma. Statistical separation into discrete populations was not possible, because the spread was continuous and the data passed the $P\chi^2$ test (Table 1). Therefore, the single grain ages could represent different populations of detrital ages that overlap within errors. Postdepositional annealing of the zircon grains to temperatures higher than 200°C is unlikely, because all zircon single grain FT ages are older than or equal to the depositional age (~59–40 Ma). Similar zircon FT single grain ages were found in the Maastrichtian sandstones in Motajica (110 to 74 Ma; Figure S5), with the difference that zircons from the Eocene sandstones are all rounded. This suggests that they could have been derived and reworked from the Sava Zone ophiolites and the Maastrichtian sandstones.

[61] A dolerite sample from the western Vardar ophiolitic complex in South Kozara (K135a; Figure 5) yielded a zircon FT age of 96 ± 22 Ma. In agreement with the observations above, this shows that neither the western Vardar ophiolitic complex nor its unconformable Paleogene cover experienced resetting of the zircon FT system during Maastrichtian thrusting, such as detected in the more internal Sava Zone units. This implies a major thrust separating the Sava Zone units and the western Vardar ophiolitic complex. Initial thrusting along this contact must be of pre-Thanetian age (most likely Maastrichtian [*Ustaszewski et al.*, 2009]), since Thanetian limestones in both North and South Kozara unconformably overlie units of contrasting paleogeographic origin. Final tectonic juxtaposition of these units took place after the Lutetian (~40 Ma).

[62] The zircon FT age of 135 ± 16 Ma obtained on a Paleozoic granite from Papuk Mountain (sample UK06-28; Figure 3) suggests that the Tisza-Dacia Mega-unit cooled to temperatures below ~200°C before all other more external units in the studied transect. This supports our interpretation that Tisza-Dacia occupied an upper plate position during end-of-Cretaceous closure of the last remnants of the Meliata-Vardar Ocean. The apatite FT central age and modeling of apatite FT data (Figure 14c) show that final cooling took place during the Eocene, similar to the hanging wall of the Motajica detachment.

[63] In conclusion and in chronological order, all structural and fission track data obtained from the hanging wall of the extensional detachment in the Sava Zone indicate cooling starting at around 60 Ma. We relate this cooling to hanging wall erosion, which accompanies thrusting of Sava Zone units onto more external units. Apatite fission track data together with modeling indicate a second cooling event starting at around 40 Ma (Figure 14), discernible in various units of different tectonostratigraphic position. The modeled fast cooling through the apatite PAZ suggests tectonic control, e.g., by accelerated hanging wall erosion following the accretion of more external units into the evolving Dinarides nappe stack. Fission track data from the footwall units of the Motajica detachment (including structurally analogous samples in Prosara and Cer Mountain) indicate a third phase of enhanced cooling during core complex formation starting 25 Ma ago and taking place within an extensional (or trans-

tensional) corridor at least 150 km long, located at the southern rim of the Pannonian basin (Figure 15).

6. Geodynamic and Thermal Evolution of the Sava Zone

[64] Maastrichtian turbiditic sandstones and shales overlying Campanian ophiolites and pelagic sediments indicate an underfilled basin (Figure 4). This possibly suggests a trench front of the advancing European plate during subduction of the remaining Mesozoic Neotethys. Provenance analysis (Figure S5) shows that detritus was predominantly shed from continental basement and volcanic edifices located in upper plate Tisza-Dacia, but also from the Sava Zone itself. The Maastrichtian siliciclastics thus date the onset of collision between the Adriatic and European plates. Our age data indicate that peak conditions during Barrovian metamorphism within the Sava Zone were reached at around 65 Ma. P-T conditions during this event reached temperatures between 550°C and 630°C and pressures between 5 and 7 kbar, corresponding to a depth of about 15 to 21 km (section 3.2). Since the Sava Zone units occupy the tectonically highest position in the nappe stack of the Dinarides, this metamorphism must have been caused by tectonic burial of the most internal slices of the Adriatic continental lithosphere underneath the Europe-derived Tisza-Dacia plate during Adria-Europe collision. More external parts of the Sava Zone, outcropping in Kozara Mountain, have experienced temperatures not much higher than 250°C during the same time span as constrained by our zircon FT data. Metamorphic overprint of a Late Cretaceous siliciclastic succession deposited on internal Dinaridic units is also reported from the Bukulja-Venčac crystalline massif and from Jastrebac in Serbia [*Marović et al.*, 2007a, 2007b], but so far neither P-T estimates nor radiometric ages are available for these two areas.

[65] The P-T estimates for the Prosara and Motajica inselbergs contrast with those reported for the LP-HT metamorphics in Moslavačka Gora [*Balen and Pamić*, 2000; *Starijaš et al.*, 2006, 2010]. Also, our radiometric ages clearly postdate cooling reported from Moslavačka Gora (83–81 Ma on hornblende, 74 Ma on white mica [*Balen et al.*, 2001]). Hence, these two metamorphic events appear unrelated. Campanian-age (around 80 Ma [*Starijaš et al.*, 2004, 2006]) LP-HT metamorphism reported from Moslavačka Gora is contemporaneous with and hence more likely related to intraoceanic magmatism within the Sava Zone [*Ustaszewski et al.*, 2009].

[66] Figure 15 illustrates the Late Cretaceous to Neogene thermal evolution of the Sava Zone largely based on our new geochronological data and apatite FT modeling results. In addition we compiled age data from exploration wells that penetrated the Neogene infill of the Sava depression ("SD" in Figure 15; see Figure 3 and Foldout 1 for the well locations and Data Set S6 for the age compilation). *Lanphere and Pamić* [1992] reported hornblende K-Ar ages of 46 ± 3.5 Ma from an amphibolite in one such well. These ages are close to our amphibole $^{40}Ar/^{39}Ar$ ages from Motajica; hence we consider the pre-Neogene basement in the Sava depression in the same structural position as the metamorphics exposed below the Motajica detachment (Foldout 1). We then assigned all data either to the footwall or the hanging wall of the Motajica detachment, analogous to the separation of our FT data. The temperature-time paths for both footwall and hanging wall show a common history of burial related to D1, starting at some time in the Maastrichtian, reaching a peak around 65 Ma followed by uniform cooling until about 40 Ma. We interpret this heating as the result of tectonic burial of the Sava Zone underneath the overriding Tisza-Dacia Mega-unit.

[67] In the case of the Motajica inselberg, the peak temperatures reached in the structurally deeper parts of the footwall are at least 300°C higher than those reached in the hanging wall, indicating substantial differential exhumation across the Motajica detachment. Zircon FT ages from the structurally highest Maastrichtian sediments of the Motajica inselberg, if at all, are only partially reset. This contrasts with the structurally deeper and fully reset hanging wall rocks of the North Kozara Mountain that were used to constrain the thermal history of the Sava Zone in general as depicted in Figure 15.

[68] Sedimentation in the Late Paleocene to Mid-Eocene basin (~59 to 40 Ma) on top of the western Vardar ophiolitic complex, cropping out in South Kozara Mountain (Figures 2, 3 and 5), starts with Thanetian shallow-water limestones that grade upsection into turbiditic sandstones (Figure 4). Deepening of the depositional environment was possibly controlled by flexural subsidence exerted by the gravitational load of an evolving nappe stack consisting of upper plate Europe-derived units and basally accreted Sava Zone units. The Paleogene deposits on top of the western Vardar ophiolitic complex thus represent a postcollisional "molasse"-type flexural foreland basin developed in front of the Sava Zone suture (Figure 16a). The external limit of these deposits marks the location of the undeformed foreland prior to the onset of thrust propagation into the external Dinarides since about 40 Ma (see *Mikes et al.* [2008] and *Korbar* [2009] for recent reviews).

[69] Apatite FT modeling suggests accelerated cooling through the apatite PAZ between about 40 and 35 Ma, possibly resulting from hanging wall erosion triggered by the above-described foreland propagation of thrusting (Figures 15 and 16a). Alternatively, this accelerated cooling could be related to postnappe extension. Late Eocene to Oligocene extension-related structures, predating the Motajica detachment, were not observed in our area of investigation, but are well known from a large part of the Balkan Peninsula to the southeast of our study area. There it is reported as back-arc extension that started in middle Eocene times as a direct consequence of delamination and rollback of the subducted Aegean slab [e.g., *Burchfiel et al.*, 2000, 2003, 2008; *Jolivet et al.*, 2003; *Kounov et al.*, 2004; *Dumurdzanov et al.*, 2005; *Schefer et al.*, 2010].

[70] The geodynamic context within which the Motajica granite was emplaced at 27 Ma is at present unclear. Our structural observations and geochronological constraints (Figure 15) suggest that its intrusion predates the D2 extensional phase; emplacement during an earlier (pre-D2, i.e., Late Eocene to Oligocene) extensional event, such as above, cannot be excluded. The onset of D2-related footwall exhumation represents a major geodynamic reorgani-

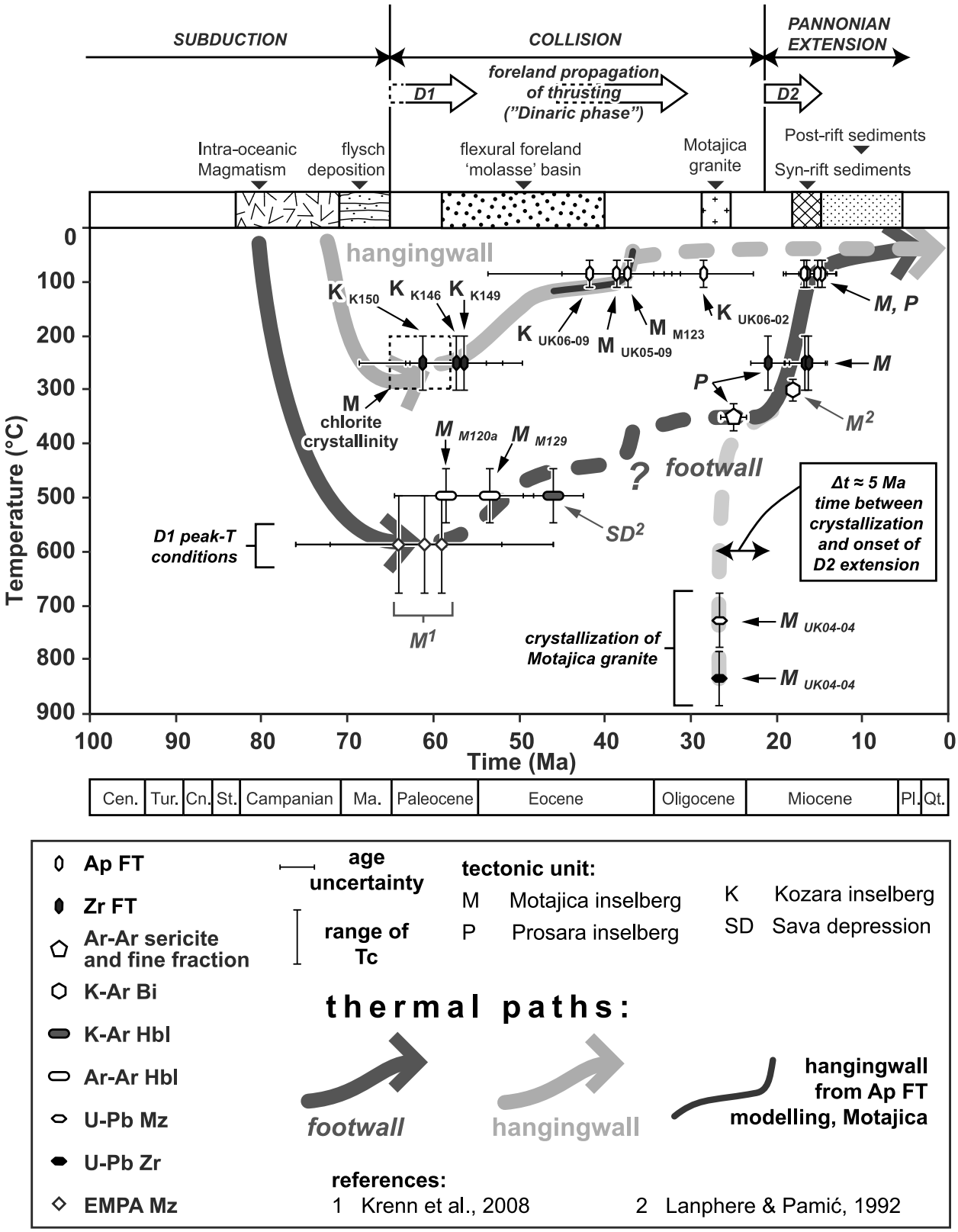

Figure 15. Temperature-time diagram showing the thermal evolution of rocks in the studied sector of the Sava Zone constrained from geochronological data derived in this study (sample number in subscripts) and from published data (superscripts). The assignment of the data to a footwall (marked by *italics*) and hanging wall relate to their tectonic position with respect to the Motajica detachment.

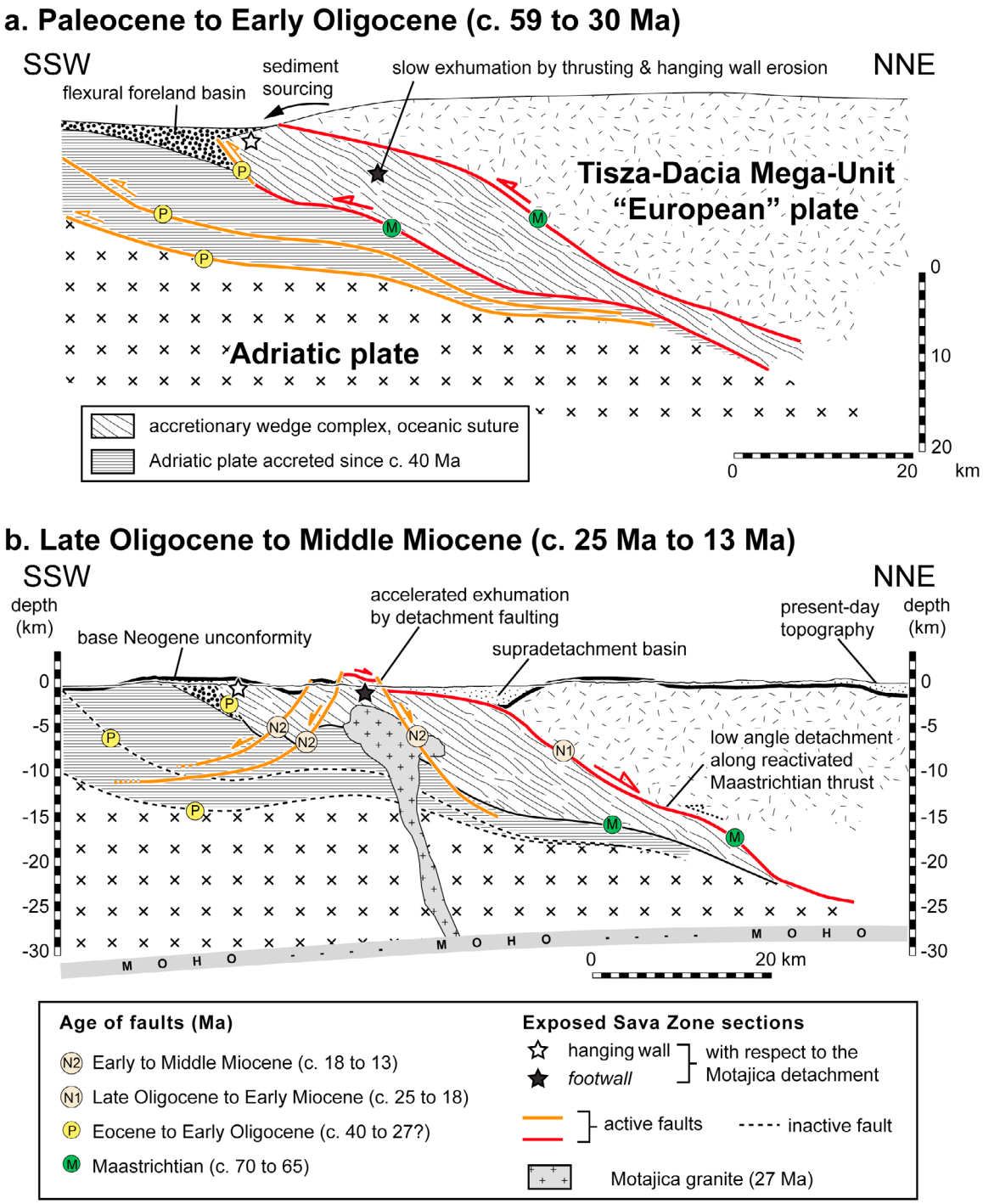

Figure 16. (a and b) Schematic sketches depicting two stages in the tectonic evolution of the Sava Zone, based on the crustal-scale transect in Foldout 1.

zation of the internal Dinarides, as it postdates major thrusts (Figure 16b). After initial rapid cooling of the Motajica granite related to its crystallization, its cooling curve joins that of the adjacent units in the footwall of the detachment. The onset of exhumation is best bracketed by the $^{40}Ar/^{39}Ar$ sericite (25 Ma) and zircon fission track ages (21 Ma) from Prosara. The later stages of cooling and exhumation of the footwall between 21 and 14 Ma are synchronous with Ottnangian to Karpatian synrift sedimentation in the Pannonian basin.

7. Transect Through the Sava Zone Suture

[71] While Foldout 1 presents an interpretative crustal-scale transect across the Sava Zone, Figure 16 schematically shows

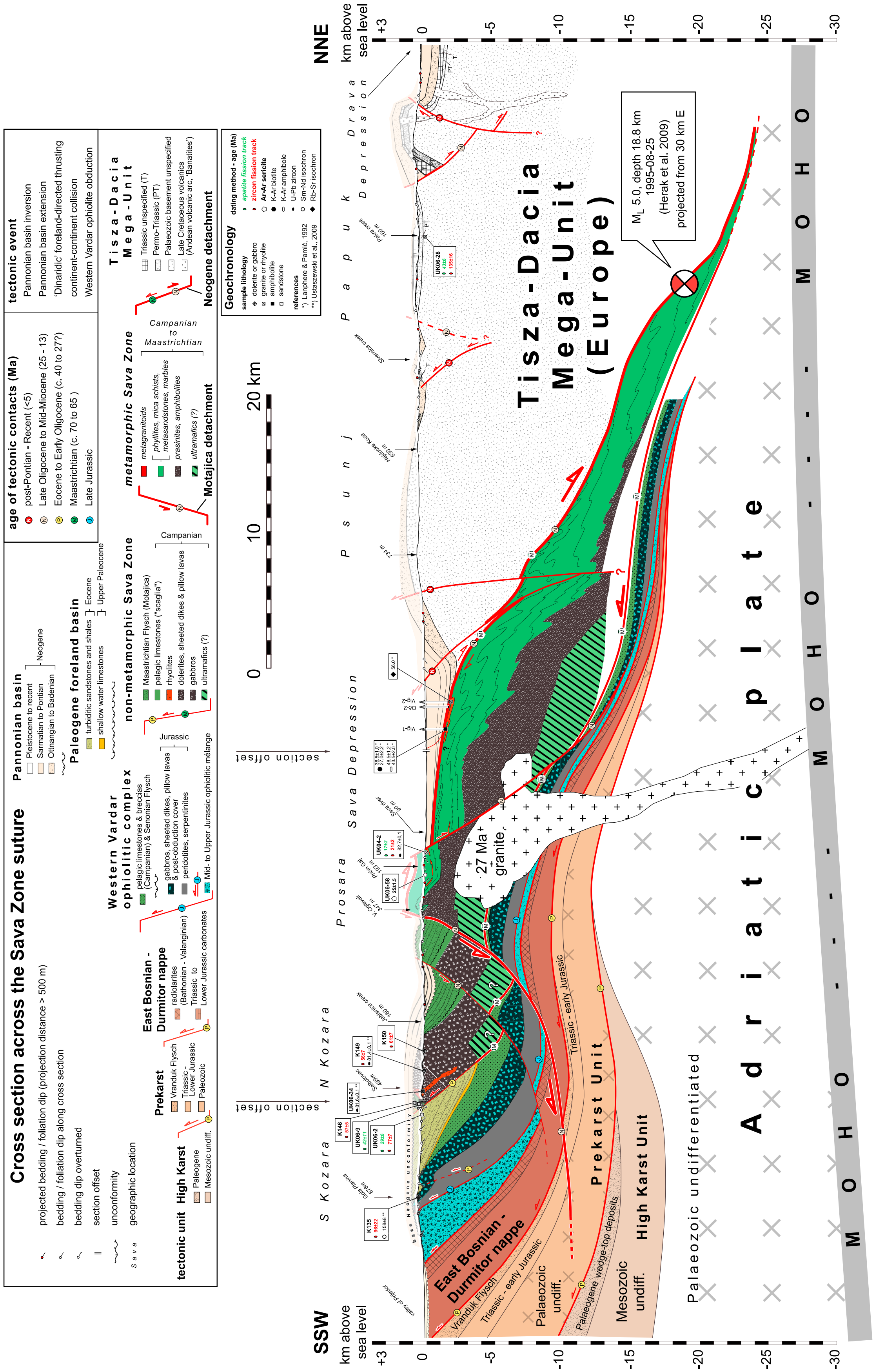

Foldout 1. Crustal-scale geological cross section across the Sava Zone. See Figures 2 and 3 for location of the section. Base of the Neogene in the Sava depression is from *Šaftić et al.* [2003]. MOHO depth is from *Horváth et al.* [2006].

two evolutionary steps of this transect. The transect hosts major thrusts associated with the formation of the Adria-Europe suture during the Maastrichtian. One such thrust juxtaposed the southern edge of the Sava Zone against the underlying western Vardar ophiolitic complex. This thrust was moderately reactivated during the Eocene (Figure 16a). Another first-order Maastrichtian thrust is inferred to have formed on top of the Sava Zone units in order to account for their observed metamorphism with a peak around 65 Ma caused by burial below Tisza-Dacia (i.e., Europe; Figure 16a). This structurally higher Maastrichtian thrust was dramatically reactivated as a major extensional detachment during Miocene core complex formation (Figure 16b and Foldout 1). We interpret the pre-Neogene basement of the Sava depression as part of the metamorphics exhumed below the Miocene detachment. The Neogene infill of the Sava depression hence represents a supradetachment basin deposited on top of the detachment [*Friedmann and Burbank*, 1995]. Motajica and Prosara are parts of one and the same metamorphic core complex that is now spatially separated by younger, brittle normal faults (Figure 6a, 7a, 7d, and 11). Compared with Motajica, Prosara exposes a shallower level of metamorphics; the detachment in Prosara is in a structurally higher position and inferred to have already been eroded. Structural evidence from Prosara shows that the Sava Zone metamorphics were exhumed below an upper plate by top-to-the-north and subordinately top-to-the-east directed sense of shear (Figure 16b). This is in line with the assumption that the upper plate units were the northerly adjacent European plate units. Later deformation in Prosara at the brittle-ductile transition is characterized by top-to-the-south tectonic transport. Inversion of the shear sense could have been caused by a reorientation of the detachment in conjunction with isostatic footwall uplift during ongoing exhumation.

[72] Foldout 1 also depicts inversion of numerous normal faults after the Pontian. This interpretation relies on both surface and reflection seismic evidence showing tilted and deformed Pontian sediments and is in agreement with earlier work in adjacent parts of the Pannonian basin suggesting compressional and/or transpressional reactivation of extensional faults [*Horváth*, 1995; *Tari and Pamić*, 1998; *Tomljenović and Csontos*, 2001; *Tomljenović*, 2002; *Saftić et al.*, 2003]. At present, the area of the southern Pannonian basin; northern Dinarides is a seismically active region with $M \geq 6$ earthquakes in the instrumental catalog [e.g., *Herak et al.*, 1995, 2009]. An M_L 5.0 earthquake along the studied transect with a reverse faulting mechanism (event 8 in Table 1 of *Herak et al.* [2009]) projects into the cross section along what we infer to be the depth continuation of the Miocene low-angle detachment. This suggests that the southern Pannonian basin is presently governed by N-S compression, in agreement with *Grenerczy et al.* [2005] and *Bada et al.* [2007].

[73] In summary, we suggest that the exhumation of Adriatic plate units in the Sava Zone from below the European plate was achieved by extensional reactivation of a Maastrichtian thrust as a low-angle detachment active from the latest Oligocene into the Middle Miocene (Figure 16b). On a larger scale this extension was linked to the synrift sedimentation of the Pannonian basin, which represents a back-arc basin related to Neogene subduction rollback in the Carpathians [e.g., *Horváth et al.*, 2006]. This back-arc extension was accompanied by substantial crustal thinning, manifested in a shallowing of the MOHO toward the Tisza-Dacia Mega-unit that initially was the upper plate during orogeny in the Dinarides (Foldout 1).

8. Conclusions

[74] We conclude the following.

[75] 1. The Sava Zone in the northern Dinarides represents a suture between the Adriatic and European plates and contains Late Cretaceous remnants of the Meliata-Vardar Ocean. These remnants were deformed into an accretionary wedge and thrust onto the distal Adriatic margin during the Maastrichtian.

[76] 2. Syncollisional tectonic burial of Adria-derived continental crust (including previously obducted western Vardar ophiolitic complex) underneath the overriding European plate gave rise to a deformation phase D1 and Barrovian metamorphism in the structurally deepest parts of the accretionary wedge. Peak temperatures between 550°C and 630°C and pressures between 5 and 7 kbar correspond to an overburden of about 15 to 21 km. Peak metamorphic conditions were most likely attained at around 65 Ma and were followed by slow and uniform cooling throughout most of the Paleogene.

[77] 3. A Late Paleocene to Mid-Eocene flexural foreland basin in front of the Sava Zone has been partly affected by deformation related to the foreland propagation of thrusting into the external Dinarides. Slightly accelerated cooling of the Sava Zone units between 40 and 35 Ma may be attributed to hanging wall erosion during this foreland propagation. Unroofing by Late Eocene to Oligocene back-arc extension, not observed in the study area due to a pre-Miocene erosional gap, but widespread elsewhere in the Balkan Peninsula, is a viable alternative and could also offer a scenario for the intrusion of the 27 Ma old Motajica two-mica granite.

[78] 4. During the Miocene the Sava Zone underwent strongly accelerated cooling related to core complex formation. The onset of this D2 extensional unroofing is bracketed by the youngest $^{40}Ar/^{39}Ar$ ages on sericites (25 Ma) and the oldest zircon FT ages (21 Ma) from the footwall of the low-angle Motajica detachment. Extension commenced at upper to midgreenschist facies conditions. Zircon and apatite FT ages from the footwall range between 21 and 14 Ma and indicate ongoing exhumation and cooling synchronous with the Ottnangian to Karpatian synrift phase of the Pannonian basin. The low-angle detachment was cut by brittle high-angle normal faults during this late stage.

[79] 5. We suggest that the extensional reactivation of a suturing Maastrichtian thrust as a low-angle detachment was responsible for the exhumation of Adriatic plate units from below the European plate. On a large scale, this extension was linked to the formation of the Pannonian back-arc basin in response to subduction in the Carpathians.

[80] 6. Late stage inversion during Pliocene to recent times led to minor high-angle reverse faulting at the northern margin of the Sava Zone and the northerly adjacent Tisza-Dacia Mega-unit.

[81] **Acknowledgments.** It is the late Jakob Pamić (Zagreb) who pioneered work on the Sava Zone inselbergs and who first introduced one of us (S. Schmid) to this key area. We devote this work to his memory. We thank Sébastien Potel (Frankfurt) for illite crystallinity measurements. The determination of the amphibole chemistry was the courtesy of Jürgen Konzett (Innsbruck). Helga Kemnitz (Potsdam) is thanked for determining the sericite chemistry. Thanks are extended to Maria Ovtcharova (Geneva) and Senecio Schefer (Basel) for U-Pb age determinations. Thorough reviews of Bruno Tomljenović (Zagreb) and two anonymous colleagues helped to further improve the manuscript. Daniel Bernoulli (Basel) and Johannes Glodny (Potsdam) provided additional helpful comments. Financial support for the Basel group through the Swiss National Science Foundation (projects "Tisza" 200021-101883/1 and 200020-109278/1) and for E.K. through the Austrian FWF (project 22480) is kindly acknowledged.

References

Árkai, P., and D. Sadek Ghabrial (1997), Chlorite crystallinity as an indicator of metamorphic grade of low-temperature meta-igneous rocks: A case study from the Bükk Mountains, northeast Hungary, *Clay Miner.*, *32*, 205–222, doi:10.1180/claymin.1997.032.2.04.

Árkai, P., F. P. Sassi, and R. Sassi (1995), Simultaneous measurements of chlorite and illite crystallinity: A more reliable tool for monitoring low- to very low grade metamorphism in metapelites—A case study from the Southern Alps (NE Italy), *Eur. J. Mineral.*, *7*, 1115–1128.

Aubouin, J., R. Blanchet, J.-P. Cadet, P. Celet, J. Charvet, J. Chorowicz, M. Cousin, and J.-P. Rampnoux (1970), Essai sur la géologie des Dinarides, *Bull. Soc. Geol. Fr.*, *12*, 1060–1095.

Bada, G., F. Horváth, P. Dövényi, P. Szafian, G. Windhoffer, and S. Cloetingh (2007), Present-day stress field and tectonic inversion in the Pannonian basin, *Global Planet. Change*, *58*, 165–180, doi:10.1016/j.gloplacha.2007.01.007.

Balen, D., and J. Pamić (2000), Crystalline complex of Mt. Moslavačka Gora, *Vijesti Hrvatskoga Geol. Drus.*, *37*, 19–22.

Balen, D., R. Schuster, and V. Garašić (2001), A new contribution to the geochronology of Mt. Moslavačka Gora (Croatia), paper DP-2 presented at PANCARDI 2001, Geod. and Geophys. Res. Inst. of the HAS, Sopron, Hungary.

Balen, D., P. Horváth, B. Tomljenović, F. Finger, B. Humer, J. Pamic, and P. Árkai (2006), A record of pre-Variscan Barrovian regional metamorphism in the eastern part of the Slavonian Mountains (NE Croatia), *Mineral. Petrol.*, *87*, 143–162, doi:10.1007/s00710-006-0120-1.

Belak, M., J. Halamić, V. Marchig, and D. Tibljas (1998), Upper Cretaceous–Palaeogene tholeiitic basalts of the southern margin of the Pannonian Basin: Požeška Gora Mt. (Croatia), *Geol. Croat.*, *51*, 163–174.

Berger, G. W., and D. York (1981), Geothermometry from dating experiments, *Geochim. Cosmochim. Acta*, *45*, 795–811, doi:10.1016/0016-7037(81)90109-5.

Berman, R. G. (1988), Internally-consistent thermodynamic data for minerals in the system Na_2O-K_2O-CaO-MgO-FeO-Fe_2O_3-Al_2O_3-SiO_2-TiO_2-H_2O-CO_2, *J. Petrol.*, *29*, 445–522.

Berza, T., E. Constantinescu, and S.-N. Vlad (1998), Upper Cretaceous magmatic series and associated mineralisation in the Carpathian-Balkan Orogen, *Resour. Geol.*, *48*, 291–306, doi:10.1111/j.1751-3928.1998.tb00026.x.

Biševac, V., D. Balen, D. Tiblaš, and D. Špahić (2009), Preliminary results on degree of thermal alteration recorded in the eastern part of Mt. Papuk, Slavonia, Croatia, *Geol. Croat.*, *62*, 63–72.

Blanchet, R. (1970), Sur un profil des Dinarides, de l'Adriatique (Split-Omiš, Dalmatie) au Bassin pannonique (Banja Luka-Doboj, Bosnie), *Bull. Soc. Geol. Fr.*, *12*, 1010–1027.

Boccaletti, M., P. Manetti, and A. Peccerillo (1974), Hypothesis on the plate tectonic evolution of the Carpatho-Balkan arcs, *Earth Planet. Sci. Lett.*, *23*, 193–198, doi:10.1016/0012-821X(74)90193-9.

Burchfiel, B. C. (1980), Eastern European Alpine system and the Carpathian orocline as an example of collision tectonics, *Tectonophysics*, *63*, 31–61, doi:10.1016/0040-1951(80)90106-7.

Burchfiel, B. C., R. Nakov, T. Tzankov, and L. Royden (2000), Cenozoic extension in Bulgaria and northern Greece: The northern part of the Aegean extensional regime, in *Tectonics and Magmatism in Turkey and the Surrounding Area*, edited by E. Bozkurt et al., *Geol. Soc. Spec. Publ.*, *173*, 325–352.

Burchfiel, B. C., R. Nakov, and T. Tzankov (2003), Evidence from the Mesta half-graben, SW Bulgaria, for the Late Eocene beginning of Aegean extension in the central Balkan Peninsula, *Tectonophysics*, *375*, 61–76, doi:10.1016/j.tecto.2003.09.001.

Burchfiel, B. C., R. Nakov, N. Dumurdzanov, D. Papanikolaou, T. Tzankov, T. Serafimovski, R. W. King, V. Kotzev, A. Todosov, and B. Nurce (2008), Evolution and dynamics of the Cenozoic tectonics of the South Balkan extensional system, *Geosphere*, *4*, 919–938, doi:10.1130/GES00169.1.

Channell, J. E. T., and F. Horváth (1976), The African/Adriatic promontory as a paleogeographical premise for Alpine orogeny and plate movements in the Carpatho-Balkan region, *Tectonophysics*, *35*, 71–101, doi:10.1016/0040-1951(76)90030-5.

Channell, J. E. T., B. D'Argenio, and F. Horváth (1979), Adria, the African promontory, in Mesozoic Mediterranean palaeogeography, *Earth Sci. Rev.*, *15*, 213–292, doi:10.1016/0012-8252(79)90083-7.

Ciobanu, C. L., N. J. Cook, and H. Stein (2002), Regional setting and geochronology of the Late Cretaceous Banatitic Magmatic and Metallogenetic Belt, *Miner. Deposita*, *37*, 541–567, doi:10.1007/s00126-002-0272-9.

Connolly, J. A. D. (2005), Computation of phase-equilibria by linear programming: A tool for geodynamic modeling and its application to subduction zone decarbonation, *Earth Planet. Sci. Lett.*, *236*, 524–541, doi:10.1016/j.epsl.2005.04.033.

Csontos, L., and A. Vörös (2004), Mesozoic plate tectonic reconstruction of the Carpathian region, *Palaeogeogr. Palaeoclimatol. Palaeoecol.*, *210*, 1–56, doi:10.1016/j.palaeo.2004.02.033.

de Capitani, C., and T. H. Brown (1987), The computation of chemical equilibrium in complex systems containing non-ideal solutions, *Geochim. Cosmochim. Acta*, *51*, 2639–2652, doi:10.1016/0016-7037(87)90145-1.

Dercourt, J., et al. (1986), Geological evolution of the Tethys belt from the Atlantic to the Pamirs since the LIAS, *Tectonophysics*, *123*, 241–315, doi:10.1016/0040-1951(86)90199-X.

Dimitrijević, M. D. (1997), *Geology of Yugoslavia*, 190 pp., Geol. Inst. GEMINI, Beograd.

Dimitrijević, M. D. (2001), Dinarides and the Vardar Zone: A short review of the geology, *Acta Vulcanol.*, *13*, 1–8.

Dumurdzanov, N., T. Serafimovski, and B. C. Burchfiel (2005), Cenozoic tectonics of Macedonia and its relation to the South Balkan extensional regime, *Geosphere*, *1*, 1–22, doi:10.1130/GES00006.1.

Filipović, I., M. Veselinović, D. Rajcević, D. Bodić, S. Petronijević, M. Rakić, N. Gagić, and M. Milicević (1967), Basic geological map sheet of Yugoslavia 1:100.000, sheet Vladimirci L34-124, Fed. Geol. Inst., Beograd.

Friedmann, S. J., and D. W. Burbank (1995), Rift basins and supradetachment basins: Intracontinental extensional end-members, *Basin Res.*, *7*, 109–127, doi:10.1111/j.1365-2117.1995.tb00099.x.

Gaidies, F., E. Krenn, C. de Capitani, and R. Abart (2008), Coupling forward modelling of garnet growth with monazite geochronology: An application to the Rappold Complex (Austroalpine crystalline basement), *J. Metamorph. Petrol.*, *26*, 775–793, doi:10.1111/j.1525-1314.2008.00787.x.

Georgiev, G., C. Dabovski, and G. Stanisheva-Vassileva (2001), East-Srednogorie–Balkan Rift Zone, in *Peri-Tethys Memoir 6: Peri-Tethyan Rift/Wrench Basins and Passive Margins*, edited by P. A. Ziegler et al., pp. 259–293, Mus. Natl. D'hist., Paris.

Gradstein, F. M., J. G. Ogg, A. G. Smith, W. Bleeker, and L. J. Lourens (2004), A new geologic time scale, with special reference to Precambrian and Neogene from the Dabie Mountains, central China, *Episodes*, *27*(2), 83–100.

Grenerczy, G., G. Sella, S. Stein, and A. Kenyeres (2005), Tectonic implications of the GPS velocity field in the northern Adriatic region, *Geophys. Res. Lett.*, *32*, L16311, doi:10.1029/2005GL022947.

Grubić, A., R. Radoičić, M. Knežević, and R. Cvijić (2009), Occurrence of Upper Cretaceous pelagic carbonates within ophiolite-related pillow basalts in the Mt. Kozara area of the Vardar zone western belt, northern Bosnia, *Lithos*, *108*, 126–130, doi:10.1016/j.lithos.2008.10.020.

Haas, J. (2001), *Geology of Hungary*, 317 pp., Eötvös Univ. Press, Budapest.

Haas, J., and C. Péró (2004), Mesozoic evolution of the Tisza Mega-unit, *Int. J. Earth Sci.*, *93*, 297–313, doi:10.1007/s00531-004-0384-9.

Handler, R., F. Neubauer, S. Velichkova, and Z. Ivanov (2004), $^{40}Ar/^{39}Ar$ age constraints on the timing of magmatism and postmagmatic cooling in the Panagyurishte region, Bulgaria, *Schweiz. Mineral. Petrogr. Mitt.*, *84*, 119–132.

Harrison, T. M., and I. McDougall (1980), Investigations of an intrusive contact, northwest Nelson, New Zealand—I. Thermal, chronological and isotopic constraints, *Geochim. Cosmochim. Acta*, *44*, 1985–2003, doi:10.1016/0016-7037(80)90198-2.

Harrison, T. M., J. Célérier, A. B. Aikman, J. Hermann, and M. T. Heizler (2009), Diffusion of ^{40}Ar in muscovite, *Geochim. Cosmochim. Acta*, *73*, 1039–1051, doi:10.1016/j.gca.2008.09.038.

Heinrich, C. A., and F. Neubauer (2002), Cu-Au-Pb-Zn-Ag metallogeny of the Alpine-Balkan-Carpathian-Dinaride geodynamic province, *Miner. Deposita*, *37*, 533–540, doi:10.1007/s00126-002-0271-x.

Herak, D., M. Herak, and B. Tomljenović (2009), Seismicity and earthquake focal mechanisms in north-western Croatia, *Tectonophysics*, *465*, 212–220, doi:10.1016/j.tecto.2008.12.005.

Herak, M., D. Herak, and S. Markušić (1995), Fault-plane solutions for earthquakes (1956–1995) in Croatia and neighbouring regions, *Geofizika*, *12*, 43–56.

Hoisch, T. D. (1990), Empirical calibration of six geobarometers for the mineral assemblage quartz + muscovite +biotite + plagioclase + garnet, *Contrib. Mineral. Petrol.*, *104*, 225–234, doi:10.1007/BF00306445.

Holland, T. J. B., and R. Powell (1998), An internally consistent thermodynamic data set for phases of petrological interest, *J. Metamorph. Geol.*, *16*, 309–343, doi:10.1111/j.1525-1314.1998.00140.x.

Horváth, F. (1995), Phases of compression during the evolution of the Pannonian Basin and its bearing on hydrocarbon exploration, *Mar. Pet. Geol.*, *12*, 837–844, doi:10.1016/0264-8172(95)98851-U.

Horváth, F., G. Bada, P. Szafián, G. Tari, A. Ádám, and S. Cloetingh (2006), Formation and deformation of the Pannonian Basin: Constraints from observation-

al data, in *European Lithosphere Dynamics*, edited by D. G. Gee and R. A. Stephenson, pp. 191–206, Geol. Soc. of London, London.

Jamičić, D. (2007), Upper Cretaceous deposits of the Požeška Gora Mt. (Croatia), *Natura Croat.*, *16*, 105–120.

Jelaska, V. (1981), Facijalne karakteristike fliša Kozare (Facial characteristics of the Mt. Kozara flysch (North Bosnia)) (in Croatian with English summary), *Vesn., Ser. A, Geol.*, *38–39*, 137–145.

Jelaska, V., J. Bulić, and E. Oreški (1970), Stratigrafski model Eocenskog fliša Banije (Stratigraphic model of Eocene flysch sediments in the Banija area) (in Croatian with English summary), *Geol. Vjesn.*, *23*, 81–94.

Jelaska, V., J. Bulić, Z. Velimirović, V. Bauer, and J. Benić (1976), Some observations on the stratigraphy of the Vučjak and Trebovac area (northern Bosnia, Yugoslavia) (in Serbian with English abstract), *Geol. Vjesn.*, *29*, 389–395.

Jolivet, L., C. Faccenna, B. Goffe, E. Burov, and P. Agard (2003), Subduction tectonics and exhumation of high-pressure metamorphic rocks in the Mediterranean orogens, *Am. J. Sci.*, *303*, 353–409, doi:10.2475/ajs.303.5.353.

Jovanović, C., and N. Magaš (1986), Basic geological map sheet of Yugoslavia 1:100.000, sheet Kostajnica L 33-106, Fed. Geol. Inst., Beograd.

Jurković, I. (2004), Metallogeny of Eocene syncollisional granites of Motajica and Prosara Mountains, *Rud. Geol. Naftni Zb.*, *16*, 31–46.

Karamata, S., J. Olujić, L. Protić, D. Milovanović, L. Vujnović, A. Popević, E. Memović, Z. Radovanović, and K. Resimić-Sarić (2000), The western belt of the Vardar Zone: The remnant of a marginal sea, in *Proceedings of the International Symposium "Geology and Metallogeny of the Dinarides and the Vardar Zone," Collect. Monogr.*, vol. 1, edited by S. Karamata and S. Janković, pp. 131–135, Acad. of Sci. and Arts of the Repub. of Srpska, Banja Luka, Bosnia.

Karamata, S., M. Sladić-Trifunović, V. Cvetković, D. Milovanović, K. Šarić, J. Olujić, and L. Vujnović (2005), The western belt of the Vardar Zone with special emphasis to the ophiolites of Podkozarje: The youngest ophiolitic rocks of the Balkan Peninsula, *Bull. Acad. Serbe Sci. Arts, Cl. Sci. Math. Nat. Sci. Nat.*, *43*, 85–96.

Kisch, H. J. (1990), Calibration of the anchizone: A critical comparison of illite "crystallinity" scales used for definition, *J. Metamorph. Geol.*, *8*, 31–46, doi:10.1111/j.1525-1314.1990.tb00455.x.

Kisch, H. J. (1991), Illite crystallinity: Recommendation on sample preparation, X-ray diffraction settings, and interlaboratory samples, *J. Metamorph. Geol.*, *9*, 665–670, doi:10.1111/j.1525-1314.1991.tb00556.x.

Knežević, V. (1962), Postanak i petrohemijski karakter magmatskih i kontaktno metamorfnih stena Cera (Origin and petrochemical characteristics of igneous and contact metamorphosed rocks of Cer Mountain) (in Serbian with English extended abstract), *Zb. Rad. Rud. Geol. Fak.*, *7*, 191–202.

Knežević, V., S. Karamata, V. Cvetković, and Z. Pécskay (1994a), Genetic groups of the enclaves in the granitic rocks of the Cer Mountain (western Serbia), *Ann. Geol. Peninsule Balk.*, *58*, 219–234.

Knežević, V., S. Karamata, and V. Cvetković (1994b), Tertiary granitic rocks along the southern margin of the Pannonian Basin, *Acta Mineral. Petrogr.*, *35*, 71–80.

Korbar, T. (2009), Orogenic evolution of the external Dinarides in the NE Adriatic region: A model constrained by tectonostratigraphy of Upper Cretaceous to Paleogene carbonates, *Earth Sci. Rev.*, *96*, 296–312, doi:10.1016/j.earscirev.2009.07.004.

Koroneos, A., G. Poli, V. Cvetković, G. Christofides, D. Krstić, and Z. Pécskay (2010), Petrogenetic and tectonic inferences from the study of the Mt Cer pluton (West Serbia), *Geol. Mag.*, doi:10.1017/S0016756810000476, in press.

Kounov, A., D. Seward, D. Bernoulli, J.-P. Burg, and Z. Ivanov (2004), Thermotectonic evolution of an extensional dome: The Cenozoic Osogovo-Lisets core complex (Kraishte zone, western Bulgaria), *Int. J. Earth Sci.*, *93*, 1008–1024, doi:10.1007/s00531-004-0435-2.

Krenn, E., and F. Finger (2004), Metamorphic formation of Sr-apatite and Sr-bearing monazite in a high-pressure rock from the Bohemian Massif, *Am. Mineral.*, *89*, 1323–1329.

Krenn, E., K. Ustaszewski, and F. Finger (2008), Detrital and newly formed metamorphic monazite in amphibolite-facies metapelites from the Motajica Massif, Bosnia, *Chem. Geol.*, *254*, 164–174, doi:10.1016/j.chemgeo.2008.03.012.

Lanphere, M., and J. Pamić (1992), K-Ar and Rb-Sr ages of Alpine granite-metamorphic complexes in the northwestern Dinarides and the southwestern part of the Pannonian Basin in northern Croatia, *Acta Geol.*, *22*, 97–111.

Laslett, G. M., P. F. Green, I. R. Duddy, and A. J. W. Gleadow (1987), Thermal annealing of fission track in apatite, 2. A quantitative analysis, *Chem. Geol.*, *65*, 1–13, doi:10.1016/0009-2541(87)90189-6.

Majer, V., and B. Lugović (1991), Metamorfne stijene s alkalnim amfibolima ("Glaukofanski škriljci") u Jugoslaviji (Metamorphic rocks with alkalic amphiboles ("glaucophane schists") in Yugoslavia)) (in Croatian with English abstract), *Rad Hrvatske Akad. Znan. Umjet.*, *458*, 103–129.

Marović, M., I. Đoković, M. Toljić, J. Milikojević, and D. Spahić (2007a), Paleogene–Early Miocene deformations of Bukulja-Venčac crystalline (Vardar Zone, Serbia), *Ann. Geol. Peninsule Balk.*, *68*, 9–20.

Marović, M., I. Đoković, M. Toljić, D. Spahić, and J. Milikojević (2007b), Extensional unroofing of the Veliki Jastrebac dome (Serbia), *Ann. Geol. Peninsule Balk.*, *68*, 21–27.

Mezger, K. (1990), Geochronology in granulites, in *Granulites and Crustal Evolution*, edited by D. Vielzeuf and P. Vidal, pp. 451–470, Kluwer Acad., Dordrecht, Netherlands.

Mikes, T., I. Dunkl, H. von Eynatten, M. Báldi-Beke, and M. Kázmer (2008), Calcareous nannofossil age constraints on Miocene flysch sedimentation in the outer Dinarides (Slovenia, Croatia, Bosnia-Hercegovina and Montenegro), in *Tectonic Aspects of the Alpine-Dinaride-Carpathian System*, edited by S. Siegesmund, B. Fügenschuh, and N. Froitzheim, *Geol. Soc. Spec. Publ.*, *298*, 335–363.

Milovanović, D., V. Marchig, and S. Karamata (1995), Petrology of the crossite schist from Fruška Gora Mts (Yugoslavia), relic of a subducted slab of the Tethyan oceanic crust, *J. Geodyn.*, *20*, 289–304, doi:10.1016/0264-3707(95)00005-T.

Mojsilović, S., I. Filipović, V. Rodin, M. Navala, D. Baklaic, and I. Đoković (1975), Basic geological map sheet of Yugoslavia 1:100.000, sheet Zvornik L34-123, Fed. Geol. Inst., Beograd.

Neubauer, F. (2002), Contrasting Late Cretaceous with Neogene ore provinces in the Alpine-Balkan-Carpathian-Dinaride collision belt, *Geol. Soc. Spec. Publ.*, *204*, 81–102.

Neubauer, F., C. A. Heinrich, and the GEODE ABCD Working Group (2003), Late Cretaceous and Tertiary geodynamics and ore deposit evolution of the Alpine-Balkan-Carpathian-Dinaride orogen, in *Mineral Exploration and Sustainable Development: Proceedings of the Seventh Biennial SGA Meeting on Mineral Exploration and Sustainable Development, Athens, Greece, August 24–28, 2003*, edited by D. G. Eliopoulos et al., pp. 1133–1136, Millpress Sci., Rotterdam, Netherlands.

Nicolescu, Ş., D. H. Cornell, and A.-V. Bojar (1999), Age and tectonic setting of Bocşa and Ocna de Fier–Dognecea granodiorites (southwest Romania) and of associated skarn mineralisation, *Miner. Deposita*, *34*, 743–753, doi:10.1007/s001260050235.

Pamić, J. (1993a), Eoalpine to Neoalpine magmatic and metamorphic processes in the northwestern Vardar Zone, the easternmost Periadriatic Zone and the southwestern Pannonian Basin, *Tectonophysics*, *226*, 503–518, doi:10.1016/0040-1951(93)90135-7.

Pamić, J. (1993b), Late Cretaceous volcanic rocks from some oil wells in the Drava depression and adjacent mountains of the southern parts of the Pannonian Basin (North Croatia), *Nafta*, *44*, 203–210.

Pamić, J. (1997), *Vulkanske Stijene Savsko-Dravskog Međuriječja i Baranje (Hrvatska)* (*Volcanic Rocks of the Sava-Drava Interfluve and Baranja (Croatia)*) (in Croatian with English summary), 192 pp., INA-Naftaplin, Zagreb.

Pamić, J. (1998), North Dinaridic Late Cretaceous–Paleogene subduction-related tectonostratigraphic units of the southern Tisia, Croatia, *Geol. Carpathica*, *49*, 341–350.

Pamić, J. (2000), Variscan crystalline complex of the Slavonian Mts, in *PANCARDI Field Trip Guide Book*, edited by J. Pamić and B. Tomljenović, pp. 48–52, Hrvatsko Geolosko Drustvo, Dubrovnik, Croatia.

Pamić, J. (2002), The Sava-Vardar Zone of the Dinarides and Hellenides versus the Vardar Ocean, *Eclogae Geol. Helv.*, *95*, 99–113.

Pamić, J., and D. Balen (2001), Tertiary magmatism of the Dinarides and the adjoining South Pannonian Basin: An overview, *Acta Vulcanol.*, *13*, 9–24.

Pamić, J., and H. Hrvatović (2000), Dinaride ophiolite zone (DOZ), in *PANCARDI 2000 Fieldtrip Guidebook*, edited by J. Pamić and B. Tomljenović, *Vijesti Hrvatskoga Geol. Drus.*, *37*, 60–68.

Pamić, J., and Z. Pécskay (1994), Geochronology of Upper Cretaceous and Tertiary igneous rocks from the Slavonija-Srijem Depression, *Nafta*, *45*, 331–339.

Pamić, J., and E. Prohić (1989), Novi prilog petrološkom poznavanju alpinskih granitnih i metamorfnih stijena Motajice u sjevernim Dinaridima u Bosni (A new contribution to the petrology of Alpine granite and metamorphic rocks from Motajica Mt. in the northernmost Dinarides, Yugoslavia) (in Serbian with English abstract), *Geol. Glas.*, *13*, 145–176.

Pamić, J., and M. Šparica (1983), The age of the volcanic rocks of Požeška Gora (Croatia, Yugoslavia) (in Croatian with English abstract), *Rad Jugosl. Akad. Znan. Umjet.*, *404*, 183–198.

Pamić, J., M. Lanphere, and E. McKee (1988), Radiometric ages of metamorphic and associated igneous rocks of the Slavonian Mountains in the southern part of the Pannonian Basin, Yugoslavia, *Acta Geol.*, *18*, 13–39.

Pamić, J., P. Árkai, J. O'Neil, and C. Antai (1992), Very low- and low-grade progressive metamorphism of Upper Cretaceous sediments of Mt. Motajica, northern Dinarides, in *Special Volume to the Problems of the Paleozoic Geodynamic Domains: Western Carpathians, Eastern Alps*, edited by J. Vozar, pp. 131–146, Dionýz Stur Inst. of Geol., Bratislava.

Pamić, J., M. Belak, T. D. Bullen, M. A. Lanphere, and E. H. McKee (2000), Geochemistry and geodynamics of a Late Cretaceous bimodal volcanic association from the southern part of the Pannonian Basin in Slavonija (northern Croatia), *Mineral. Petrol.*, *68*, 271–296, doi:10.1007/s007100050013.

Pamić, J., D. Balen, and M. Herak (2002), Origin and geodynamic evolution of Late Paleogene magmatic associations along the Periadriatic-Sava-Vardar magmatic belt, *Geodin. Acta*, *15*, 209–231, doi:10.1016/S0985-3111(02)01089-6.

Pantić, N., and O. Jovanović (1970), O starosti "azoika" ili "paleozoijskih skriljaca" na Motajici na osnovu mikrofloristickih podatka (On the age of "Azoic" or "Palaeozoic" slates in Motajica Mountain based on microfloristic remnants) (in Serbian with English abstract), *Geol. Glas.*, *14*, 190–214.

Pavelić, D. (2001), Tectonostratigraphic model for the North Croatian and North Bosnian sector of the Miocene Pannonian Basin system, *Basin Res.*, *13*, 359–376, doi:10.1046/j.0950-091x.2001.00155.x.

Ricou, L. E., J. Dercourt, J. Geyssant, C. Grandjacquet, C. Lepvrier, and B. Biju-Duval (1986), Geological constraints on the Alpine evolution of the Mediterranean Tethys, *Tectonophysics*, *123*, 83–86, 89–122, doi:10.1016/0040-1951(86)90194-0.

Rieser, A. B., F. Neubauer, R. Handler, S. H. Velichkova, and Z. Ivanov (2008), New $^{40}Ar/^{39}Ar$ age constraints on the timing of magmatic events in the Panagyurishte

region, Bulgaria, Swiss *J. Geosci.*, *101*, 107–123, doi:10.1007/s00015-007-1243-z.

Saftić, B., J. Velić, O. Sztanó, G. Juhász, and Ž. Ivković (2003), Tertiary subsurface facies, source rocks and hydrocarbon reservoirs in the SW part of the Pannonian Basin (northern Croatia and south-western Hungary), *Geol. Croat.*, *56*, 101–122.

Săndulescu, M. (1984), *Geotectonica României* (*Geotectonics of Romania*), 450 pp., Ed. Teh., Bucharest.

Schefer, S., B. Fügenschuh, S. M. Schmid, D. Egli, and K. Ustaszewski (2007), Tectonic evolution of the suture zone between Dinarides and Carpatho-Balkan: Field evidence from the Kopaonik region, southern Serbia, *Geophys. Res. Abstr.*, *9*, abstract 03891.

Schefer, S., D. Egli, W. Frank, B. Fügenschuh, M. Ovtcharova, U. Schaltegger, B. Schoene, and S. M. Schmid (2008), Metamorphic and igneous evolution of the innermost Dinarides in Serbia, paper presented at 6th Swiss Geoscience Meeting, Swiss Acad. of Sci., Lugano, Switzerland.

Schefer, S., V. Cvetković, B. Fügenschuh, A. Kounov, M. Ovtcharova, U. Schaltegger, and S. M. Schmid (2010), Cenozoic granitoids in the Dinarides of southern Serbia: Age of intrusion, isotope geochemistry, exhumation history and significance for the geodynamic evolution of the Balkan Peninsula, *Int. J. Earth Sci.*, doi:10.1007/s00531-010-0599-x, in press.

Schmid, S. M., D. Bernoulli, B. Fügenschuh, L. Matenco, R. Schuster, S. Schefer, M. Tischler, and K. Ustaszewski (2008), The Alpine-Carpathian-Dinaridic orogenic system: Correlation and evolution of tectonic units, *Swiss J. Geosci.*, *101*, 139–183, doi:10.1007/s00015-008-1247-3.

Šparica, M., and J. Pamić (1986), Prilog poznavanju tektonike Požeške Gore u Slavoniju (A contribution to the knowledge of tectonics of Mt. Požeška Gora in Slavonia) (in Croatian with English abstract), *Rad Jugosl. Akad. Znan. Umjet.*, *424*, 85–96.

Šparica, M., R. Bužaljko, and C. Jovanović (1980), Basic geological map sheet of Yugoslavia 1:100.000, sheet Nova Kapela L 33-108, Fed. Geol. Inst., Beograd.

Šparica, M., R. Bužaljko, and C. Jovanović (1984), Basic geological map sheet of Yugoslavia 1:100.000, sheet Nova Gradiska L 33-107, Fed. Geol. Inst., Beograd.

Stampfli, G. M., and G. D. Borel (2002), A plate tectonic model for the Paleozoic and Mesozoic constrained by dynamic plate boundaries and restored synthetic oceanic isochrons, *Earth Planet. Sci. Lett.*, *196*, 17–33, doi:10.1016/S0012-821X(01)00588-X.

Starijaš, B., D. Balen, D. Tiblaš, R. Schuster, B. Humer, and F. Finger (2004), The Moslavačka Gora Massif in Croatia: Part of a Late Cretaceous high-heat-flow zone in the Alpine-Balkan-Carpathian-Dinaride collision belt, in *Pangeo Austria 2004: Erdwissenschaften und Öffentlichkeit, Graz*, edited by B. Hubmann, *Ber. Inst. Erdwiss. Karl-Franzens Univ. Graz*, 9, 453–454.

Starijaš, B., A. Gerdes, D. Balen, D. Tibljaš, R. Schuster, A. Mazer, B. Humer, and F. Finger (2006), Geochronology, metamorphic evolution and geochemistry of granitoids of the Moslavačka Gora Massif (Croatia), paper presented at 18th Congress of the Carpathian-Balkan Geological Association, Serb. Comm. of the CBGA, Beograd.

Starijaš, B., A. Gerdes, D. Balen, D. Tiblaš, and F. Finger (2010), The Moslavačka Gora crystalline massif in Croatia: A Cretaceous heat dome within remnant Ordovician granitoid crust, Swiss *J. Geosci.*, *103*, 61–82, doi:10.1007/s00015-010-0007-3.

Stipp, M., H. Stünitz, R. Heilbronner, and S. M. Schmid (2002), Dynamic recrystallization of quartz: Correlation between natural and experimental conditions, in *Deformation Mechanisms, Rheology, and Tectonics: Current Status and Future Perspectives*, edited by S. De Meer et al., *Geol. Soc. Spec. Publ.*, *200*, 171–190.

Tari, V., and J. Pamić (1998), Geodynamic evolution of the northern Dinarides and the southern part of the Pannonian Basin, *Tectonophysics*, *297*, 269–281, doi:10.1016/S0040-1951(98)00172-3.

Tomljenović, B. (2002), Strukturne Znacajke Medvednice i Samoborskoj gorja (Structural characteristics of Medvednica and Samoborsko gorje Mts.), Ph.D. thesis, 208 pp., Zagreb Univ., Zagreb.

Tomljenović, B., and L. Csontos (2001), Neogene-Quaternary structures in the border zone between Alps, Dinarides and Pannonian Basin (Hrvatsko Zagorje and Karlovac basins, Croatia), *Int. J. Earth Sci.*, *90*, 560–578, doi:10.1007/s005310000176.

Ustaszewski, K., S. M. Schmid, B. Fügenschuh, M. Tischler, E. Kissling, and W. Spakman (2008), A map-view restoration of the Alpine-Carpathian-Dinaridic system for the Early Miocene, *Swiss J. Geosci.*, *101*, suppl. 1, 273–294, doi:10.1007/s00015-008-1288-7.

Ustaszewski, K., S. M. Schmid, B. Lugović, R. Schuster, U. Schaltegger, D. Bernoulli, L. Hottinger, A. Kounov, B. Fügenschuh, and S. Schefer (2009), Late Cretaceous intra-oceanic magmatism in the internal Dinarides (northern Bosnia and Herzegovina): Implications for the collision of the Adriatic and European plates, *Lithos*, *108*, 106–125, doi:10.1016/j.lithos.2008.09.010.

Varičak, D. (1966), Petrološka studija motajickog granitnog masiva (Petrological study of the Motajica granite massif) (in Serbian with English abstract), Ph.D. thesis, 170 pp., Univ. of Sarajevo, Sarajevo.

Vishnevskaya, V. S., N. Djeric, and G. S. Zakariadze (2009), New data on Mesozoic radiolaria of Serbia and Bosnia, and implications for the age and evolution of oceanic volcanic rocks in the central and northern Balkans, *Lithos*, *108*, 72–105, doi:10.1016/j.lithos.2008.10.015.

von Cotta, B. (1864), Über Eruptivgesteine und Erzlagerstätten im Banat und in Serbien, 105 pp., V. Braunmüller, Vienna.

von Quadt, A., R. Moritz, I. Peytcheva, and C. A. Heinrich (2005), 3: Geochronology and geodynamics of Late Cretaceous magmatism and Cu-Au mineralization in the Panagyurishte region of the Apuseni-Banat-Timok-Srednogorie belt, Bulgaria, *Ore Geol. Rev.*, *27*, 95–126, doi:10.1016/j.oregeorev.2005.07.024.

Warr, L. N., and A. Rice (1994), Interlaboratory standardization and calibration of clay mineral crystallinity and crystallite size data, *J. Metamorph. Geol.*, *12*, 141–152, doi:10.1111/j.1525-1314.1994.tb00010.x.

Zelic, M., N. Levi, A. Malasoma, M. Marroni, L. Pandolfi, and B. Trivic (2010), Alpine tectono-metamorphic history of the continental units from Vardar zone: The Kopaonik Metamorphic Complex (Dinaric-Hellenic belt, Serbia), *Geol. J.*, *45*, 59–77, doi:10.1002/gj.1169.

Zimmerman, A., H. J. Stein, J. L. Hannah, D. Koželj, K. Bogdanov, and T. Berza (2008), Tectonic configuration of the Apuseni-Banat-Timok-Srednogorie belt, Balkans–South Carpathians, constrained by high precision Re-Os molybdenite ages, *Miner. Deposita*, *43*, 1–21, doi:10.1007/s00126-007-0149-z.

W. Frank, Central European Argon Laboratory, Geological Institute, Slovak Academy of Sciences, SK-84005 Bratislava, Slovakia. (frank.w-ceal@inmail.sk)

B. Fügenschuh, Geological-Paleontological Institute, A-6020 Innsbruck, Austria. (bernhard.fuegenschuh@uibk.ac.at)

A. Kounov, Institute of Geology and Paleontology, University of Basel, CH-4056 Basel, Switzerland. (a.kounov@unibas.ch)

E. Krenn, Division of Mineralogy, Department of Materials Science and Physics, University of Salzburg, A-5020 Salzburg, Austria. (erwin.krenn@sbg.ac.at)

U. Schaltegger, Department of Mineralogy, University of Geneva, CH-1205 Genève, Switzerland. (urs.schaltegger@terre.unige.ch)

S. M. Schmid, Institute of Geophysics, ETH Zurich, Sonneggstr. 5, CH-8092 Zurich, Switzerland. (stefan.schmid@erdw.ethz.ch)

K. Ustaszewski, Lithosphere Dynamics, GFZ German Research Centre for Geosciences, D-14473 Potsdam, Germany. (kamilu@gfz-potsdam.de)